

1 **Title:** Multi-species genome-wide CRISPR screens identify conserved suppressors of cold-
2 induced cell death

3

4 **Authors**

5 Breanna Lam^{1,*}, Kathrin M. Kajderowicz^{1,2,*}, Heather R. Keys¹, Julian M. Roessler¹, Evgeni M.
6 Frenkel¹, Adina Kirkland¹, Punam Bisht¹, Mohamed A. El-Brolosy^{1,3}, Rudolf Jaenisch¹, George
7 W. Bell¹, Jonathan S. Weissman¹, Eric C. Griffith⁴, Sinisa Hrvatin^{1,†}

8

9 **Affiliations**

10 ¹Whitehead Institute for Biomedical Research and Department of Biology, Massachusetts
11 Institute of Technology, Cambridge, MA 02142, USA

12 ²Department of Brain and Cognitive Sciences, Massachusetts Institute of Technology,
13 Cambridge, MA 02142, USA

14 ³Harvard Society of Fellows, Cambridge, MA, 02138, USA

15 ⁴Department of Neurobiology, Harvard Medical School, Boston, MA 02115, USA

16 *These two authors contributed equally to this work

17

18 **Corresponding author**

19 †Sinisa Hrvatin (shrvatin@wi.mit.edu)

20

21 **Summary**

22 Cells must adapt to environmental changes to maintain homeostasis. One of the most striking
23 environmental adaptations is entry into hibernation during which core body temperature can
24 decrease from 37°C to as low as 4°C. How mammalian cells, which evolved to optimally function
25 within a narrow range of temperatures, adapt to this profound decrease in temperature remains
26 poorly understood. In this study, we conducted the first genome-scale CRISPR-Cas9 screen in
27 cells derived from Syrian hamster, a facultative hibernator, as well as human cells to investigate
28 the genetic basis of cold tolerance in a hibernator and a non-hibernator in an unbiased manner.
29 Both screens independently revealed glutathione peroxidase 4 (GPX4), a selenium-containing
30 enzyme, and associated proteins as critical for cold tolerance. We utilized genetic and
31 pharmacological approaches to demonstrate that GPX4 is active in the cold and its catalytic
32 activity is required for cold tolerance. Furthermore, we show that the role of GPX4 as a
33 suppressor of cold-induced cell death extends across hibernating species, including 13-lined
34 ground squirrels and greater horseshoe bats, highlighting the evolutionary conservation of this

35 mechanism of cold tolerance. This study identifies GPX4 as a central modulator of mammalian
36 cold tolerance and advances our understanding of the evolved mechanisms by which cells
37 mitigate cold-associated damage—one of the most common challenges faced by cells and
38 organisms in nature.

39

40 **Introduction**

41 Rapid temperature changes pose a challenge to all clades of life, including endotherms.
42 Homeotherms such as mammals routinely defend a core body temperature set-point, with
43 profound thermal deviations leading to organ dysfunction and death¹⁻⁴. Indeed, several studies
44 have shown that while homeotherm-derived cells typically possess a capacity for mild cold
45 tolerance in culture, primary cultured cells and cell lines derived from a number of mammalian
46 species, including humans, exhibit high rates of cell death following prolonged severe cold
47 exposure⁵⁻⁸. Although considerable work has focused on understanding the cellular responses
48 and adaptations to an increased temperature (heat stress and heat-shock)⁹⁻¹¹, little is known
49 about how cell biological processes modulate cell sensitivity to decreased temperatures.

50

51 The mechanisms underlying cold-induced death remain poorly understood but have been
52 hypothesized to involve phase transition of cellular membranes, with the resulting membrane
53 damage leading to ion gradient disruption and irrecoverable cellular dysfunction¹²⁻¹⁵. However,
54 many warm-blooded animals, including some primates, have evolved the ability to enter torpor
55 and hibernation – states during which body temperature can decrease far below its homeostatic
56 set-point¹⁶⁻¹⁸. In many animals, *torpor* is a state of profoundly reduced metabolic rate and body
57 temperature lasting from hours to days, while *hibernation* is a seasonal behavior comprising
58 multiple bouts of *torpor* interrupted by periodic arousals to normal body temperature. During
59 torpor, the core body temperature of many small hibernators including the Syrian golden hamster
60 (*Mesocricetus auratus*), the 13-lined ground squirrel (*Ictidomys tridecemlineatus*), and the greater
61 horseshoe bat (*Rhinolophus ferrumequinum*), reaches 4-10°C¹⁹⁻²¹. Animals can remain at these
62 low temperatures for extended periods of time (up to several weeks), indicating that their cells
63 and tissues are either genetically predisposed to cold tolerance, or that they can adapt to tolerate
64 long-term cold exposure¹⁹⁻²².

65

66 Although in principle the ability to tolerate cold temperatures could be conveyed by systemic
67 factors present in torpid or hibernating animals, cell lines derived from hibernating rodents
68 maintain high viability when exposed to 4°C for several days, indicating the presence of cell-

69 intrinsic mechanisms of cold tolerance⁵⁻⁸. Several studies have reported distinctive responses of
70 hibernator-derived cells in the cold. For example, Syrian hamster-derived epithelial-like hamster
71 kidney (HaK) cells maintain mitochondrial membrane potential and ATP production during cold
72 exposure⁷, and both HaK and epithelial-like smooth muscle cells derived from the Syrian golden
73 hamster are able to prevent excess reactive oxygen species damage in response to cold
74 exposure⁵. Similarly, unlike human induced pluripotent stem cell (iPSC)-derived neurons, cultures
75 of iPSC-derived neurons from 13-lined ground squirrels retain microtubule stability in the cold⁶.
76 Despite metabolic and cell biological differences between various hibernator and non-hibernator-
77 derived cells in the context of cold exposure, the underlying genetic modulators of cold tolerance
78 have yet to be systematically explored. Additionally, it is still unknown to what extent the pathways
79 that regulate cold tolerance in one hibernating species are conserved across other evolutionarily
80 distant hibernators and potentially even present in non-hibernators.

81
82 Here, we carry out the first unbiased genome-scale CRISPR-Cas9 screens in cells derived from
83 a cold-tolerant hibernator (Syrian hamster) as well as human (non-hibernator) cells to identify
84 genetic pathways required for long-term cold tolerance. Surprisingly, these screens independently
85 identify a common mechanism dependent on the selenocysteine-containing enzyme Glutathione
86 Peroxidase 4 (GPX4) as a key mediator of cellular cold tolerance. Employing genetic and
87 pharmacological approaches, we confirm these findings and demonstrate that increased GPX4
88 activity is sufficient to improve cold tolerance in human cells. We further show that functional
89 GPX4 is required for cold tolerance across several hibernating and non-hibernating mammals,
90 including in distantly related hibernating horseshoe bats (*Rhinolophus ferrumequinum*), and
91 propose that the GPX4 pathway may be a widespread, evolutionarily ancient metazoan
92 mechanism of cold tolerance across endotherms.

93

94 **Results**

95

96 **Assay for measuring viability of cold-exposed cells**

97 Our initial evaluation of the ability of human K562 leukemia cells to tolerate prolonged exposure
98 to extreme cold (4°C) temperatures led us to establish a new method for assessing viability of
99 cold-exposed cells. To avoid confounding changes in media composition or pH, we transferred
100 cultured cells into incubators cooled to 4°C with the CO₂ concentration calibrated to maintain
101 physiological pH (7.4). Cell survival was assessed based on exclusion of trypan blue, a
102 membrane-impermeable dye, immediately upon removal from 4°C. We observed a 27 ± 3%

103 survival rate for K562 cells following 24 hours at 4°C using this approach. However, recounting
104 live cells after a 24-hour rewarming at 37°C revealed a ~6-fold increase in live cells, inconsistent
105 with the reported 16-24 hour doubling rate of this cell line (**Figure 1b, Figure S1a**). Reasoning
106 that a substantial fraction of trypan blue-positive cells at 4°C remain alive and capable of cell
107 division and recovery upon rewarming, we carried out a time course of trypan blue staining shortly
108 after removal from 4°C (**Figure 1a**). We found that the fraction of trypan blue-positive cells
109 dramatically reduced following a brief rewarming period (30 minutes to 1 hour, either at room
110 temperature or at 37°C), consistent with the number of live cells observed after 24 hours of
111 rewarming (**Figure 1b,c, Figure S1a,b**). To determine whether this effect was isolated to K562
112 cells, we measured trypan blue-positive cells at 4°C or following a brief period of rewarming in
113 several human cell lines (HEK 293T, HeLa, and RPE1 cells), as well as Syrian hamster kidney
114 fibroblasts (BHK-21 cells) (**Figure S1c-f**). We consistently observed that, absent a rewarming
115 period, trypan blue staining significantly overestimates cold-induced cell death. We thus adopted
116 this brief rewarming period (~30-minutes) as a standard assay to measure cell viability of cold-
117 exposed cells in our subsequent studies.

118

119 **Hibernator-derived cells show enhanced cold tolerance compared to human cells**

120 Using our modified assay for cell viability after cold challenge, we examined the relative cold
121 tolerance of hibernator and non-hibernator cells. We tested four commonly used human cell lines
122 (HT1080, HeLa, RPE1, and K562), as well as two cell lines (BHK-21 and HaK) derived from
123 Syrian hamsters (*Mesocricetus auratus*), a hibernating mammal. Cells were placed at 4°C - the
124 lower end of the temperature range which Syrian hamsters reach during hibernation - and we
125 assessed cell survival after 1, 4, and 7 days of cold exposure. Consistent with prior reports^{5,7,8},
126 hamster-derived cell lines maintained high levels of viability, whereas human cell lines showed
127 varying degrees of death (**Figures 1d-f**), with several exhibiting less than 50% survival following
128 7 days in the cold. Notably, we observed generally higher cell survival rates than previously
129 reported⁵, likely owing to our modified method of measuring cell viability. Similar survival trends
130 were also observed using an orthogonal assay based on lactate dehydrogenase (LDH) release
131 from dead cells into the media (**Figure 1g**).

132

133 **Genome-scale CRISPR screen in a hibernator-derived cell line identifies suppressors of** 134 **cold-induced cell death**

135 To investigate the molecular pathways regulating cold resistance in hibernator-derived BHK-21
136 cells, we designed a genome-scale CRISPR-Cas9 screen. Taking advantage of a recent

137 chromosome-level assembly of the *Mesocricetus auratus* genome²³ and a modified CRISPOR-
138 based guide selection algorithm (Methods), we generated a library of 218,143 single guide RNAs
139 (sgRNAs) targeting all 21,473 annotated genes (~10 guides per gene), including 2,299 intergenic-
140 targeting and 250 non-targeting sgRNAs as negative controls. The pooled library was introduced
141 into BHK-21 cells via a lentiviral vector expressing the sgRNA along with Cas9, achieving ~1000-
142 fold library representation with a multiplicity of infection (MOI) < 1.

143
144 Considering that many mammalian species, including Syrian hamsters, undergo prolonged
145 periods of cold exposure (deep torpor) and rewarming (interbout arousals) during seasonal
146 hibernation, we sought to recapitulate these temperature changes in our screen. We thus exposed
147 BHK-21 cells to three cycles consisting of 4°C cold exposure (4 days) followed by rewarming at
148 37°C (2 days) (“4°C Cycling”, **Figure 2a**). To isolate genes selectively required upon cold
149 exposure, we also analyzed BHK-21 cultures transduced in parallel that were maintained at 37°C
150 for four passages/cycles (“37°C Control”, **Figure 2a**). For both paradigms, genomic DNA was
151 isolated from cells during each cycle/passage to monitor selective sgRNA depletion. To assess
152 our screen performance, we tested whether sgRNAs targeting previously identified human core
153 essential genes²⁴ were significantly depleted compared with nontargeting and intergenic sgRNAs
154 and found that we can robustly distinguish between these functional categories at all three cycles
155 and at both 37°C and 4°C (estimated p-value < 2.2e-16) (**Figure S2**).

156
157 To identify genes that selectively modify (suppress or potentiate) cold-induced cell loss, we
158 compared the guides depleted during three cycles of cold exposure and rewarming to controls at
159 37°C with matched population doublings. Among the 21,473 targeted genes, only one gene,
160 ribosomal protein S29 (Rps29)²⁵, was selectively required in control 37°C conditions and only nine
161 genes appeared selectively required during cold exposure (FDR < 0.1, log2 fold-change [Log2FC]
162 >1, **Figure 2b, Table S1, S2**). Four selectively required genes - *Dld*, *Lias*, *Lipt1*, and *Ybey* – are
163 involved in lipoylation and mitochondrial RNA processing^{26–29}. Strikingly, five of the nine required
164 genes - *Gpx4*, *Eefsec*, *Pstk*, *Secisbp2*, and *Sepsecs* - represent known components of the
165 glutathione/Glutathione Peroxidase 4 (GPX4) antioxidant pathway, indicating that this pathway
166 functions as a potent suppressor of cold-induced cell death in hibernator-derived BHK-21 cells
167 (**Figure 2c**).

168
169 *Gpx4* encodes a selenocysteine-containing lipid antioxidant enzyme that acts to suppress lipid
170 peroxidation via the glutathione-mediated reduction of lipid hydroperoxides to non-toxic lipid

171 alcohols³⁰. GPX4 inhibition sensitizes cells to ferroptosis, a distinct form of programmed cell death
172 characterized by iron-dependent accumulation of lipid peroxidation³¹. Notably, cold exposure has
173 previously been associated with increased lipid peroxidation and ferroptosis in human cells⁵.
174 Underscoring the requirement for Gpx4 activity, four of the eight remaining genes selectively
175 required upon cold exposure (*Eefsec*, *Secisbp2*, *Pstk*, *Sepsecs*) are directly or indirectly involved
176 in selenocysteine incorporation into cellular proteins and thus required for Gpx4 activity (**Figures**
177 **2d-h**)^{32,33}.

178
179 Given that our initial screen design involved repeated rewarming cycles, we could not exclude the
180 possibility that the Gpx4 pathway confers resistance to rewarming-associated stress rather than
181 cold tolerance per se. To address this issue, we took advantage of the high cold tolerance of BHK-
182 21 cells and included a second screen arm using similar methods in which cells were continuously
183 exposed to 4°C for 15 days (**Figure 2i**). Sequencing prior to and following 15 days of cold
184 exposure, followed by a brief rewarming to 37°C, confirmed significant depletion (FDR < 0.1,
185 Log2FC < -0.5) of sgRNAs targeting *Gpx4*, *Eefsec*, and *Secisbp2* (as well as a trend toward
186 depletion for *Sepsecs* and *Pstk*), confirming a critical role for the Gpx4 pathway in BHK-21 cell
187 prolonged cold tolerance (**Figures 2j,k, Table S2, S3**). Thus, two unbiased genome-scale screen
188 arms identified Gpx4 as a major suppressor of cold-induced cell death in hibernator-derived BHK-
189 21 cells in the context of both cyclical and continuous cold exposure.

190
191 **Gpx4 catalytic activity is essential for hibernator cell survival during cold exposure**
192 To further validate the role of GPX4 in cold-mediated cell death, we employed the top-ranked
193 sgRNA from our screen to generate clonal *Gpx4* knockout BHK-21 cells. We sorted individual
194 cells to obtain clonal knockout cell lines and maintained them in the presence of liproxstatin-1
195 since they showed stunted growth at 37°C (**Figure S4a**). We confirmed the absence of Gpx4 via
196 immunoblotting (**Figure 3a**). While wild-type (WT) BHK-21 cells maintained high cell viability at
197 4°C, all three *Gpx4* knockout lines exhibited complete cell death within 4 days of cold exposure
198 (*****P* < 0.0001) (**Figure 3a**). Moreover, these differences reflected Gpx4 loss, as opposed to
199 off-target effects insofar as lentiviral re-expression of cytosolic hamster Gpx4 (*****P* < 0.0001),
200 but not a GFP control gene or a catalytically dead mutant form of Gpx4 (mGPX4) that has a
201 serine in the active site instead of a selenocysteine, restored cold tolerance of *Gpx4* knockout
202 lines (**Figures 3b,c**).

203

204 Together, these genetic experiments strongly implicate the catalytic activity of Gpx4 in BHK-21
205 cold tolerance. However, the constitutive nature of these interventions precluded a determination
206 of whether Gpx4 functions to actively oppose cell death during cold-exposure or whether loss of
207 its catalytic activity prior to cold exposure sensitizes cells to subsequent cold challenge. To
208 address this issue, we used RSL3 and ML162, two competitive small-molecule Gpx4 inhibitors^{34–}
209 ³⁶. Acute treatment of cultured BHK-21 cells with these inhibitors during cold exposure yielded
210 dose-dependent increases in cell death. Indeed, by four days of treatment, both RSL3- and
211 ML162-treated BHK-21 cells display significantly increased cold-induced death compared to
212 untreated controls ($****P < 0.0001$) (**Figures 3d,e**). Importantly, relative to WT cells, *Gpx4*
213 knockout cells exhibited no significant increase in cold-induced cell death upon RSL3 treatment
214 following a short cold exposure (8 hours) (**Figure S3**), confirming the specificity of these inhibitors
215 under the test conditions. We therefore conclude that Gpx4 catalytic activity is required in BHK-
216 21 cells during the course of cold exposure to actively oppose cold-induced cell death.

217
218 Given that Gpx4 activity acts as a major endogenous suppressor of ferroptosis³¹, we tested
219 whether the cold-induced cell death observed under Gpx4 inhibition occurred via the ferroptosis
220 pathway. To this end, we made use of two small molecule inhibitors of ferroptosis, ferrostatin-1,
221 a lipophilic antioxidant, and deferoxamine mesylate (DFO), a Fe²⁺ chelator. Both inhibitors
222 effectively rescued cold-induced cell death in the presence of the Gpx4 inhibitor RSL3 (**Figure**
223 **3f**), indicating that acute inhibition of Gpx4 activity in the cold drives cell death via ferroptosis.
224 Together, through a combination of genetic and pharmacological approaches, our studies
225 demonstrate that Gpx4 activity confers substantial cold resistance in hibernator-derived cells,
226 protecting cells from cold-induced ferroptosis.

227 228 **Genome-scale CRISPR screen identifies determinants of cold sensitivity in human cells**

229 In contrast to hibernator-derived cell lines, human cells display varying cold sensitivities in
230 culture, with some exhibiting pronounced intolerance to the cold (**Figure 1d-g**). Consistent with
231 prior reports^{5,8,37}, pharmacological experiments in several human cell lines (K562, HT1080,
232 RPE, and HeLa cells) confirmed that cold-induced cell-loss occurred primarily via ferroptosis,
233 with both antioxidant ferroptosis inhibitors (ferrostatin-1 and liproxstatin-1) and iron chelators
234 (DFO and 2'2'-pyridine) increasing the cold survival in all four cell lines in a dose-dependent
235 manner. By contrast, neither the Caspase inhibitor Z-VAD-FMK nor the necroptosis inhibitor
236 necrostatin-1 significantly affected cell viability (**Figure S5, S6**).

237

238 To gain further insight into the genetic modifiers of human cell cold sensitivity and resistance,
239 we designed and performed an additional CRISPR-Cas9 screen in cold-sensitive human K562
240 cells exposed to cold temperatures. A pooled lentiviral CRISPR-Cas9 library targeting 19,381
241 genes (~5 sgRNAs per gene) was delivered to K562 cells at an MOI of ~0.5. Transduced cells
242 were placed at 4°C for five days to allow for cold-induced cell death to occur in approximately 79
243 \pm 1.76% of cells, followed by a three-day rewarming to 37°C to allow for amplification of
244 remaining cells (**Figure 4a**). This cold-rewarming cycle was repeated three times, with cells
245 collected after each cycle to monitor the relative enrichment and depletion of individual sgRNAs.
246 As in our prior screens, separate cultures transduced in parallel were maintained at 37°C for
247 comparative analysis. In addition, to discriminate between ferroptosis-dependent and -
248 independent regulators of cold tolerance, we conducted a parallel screen in cold-exposed K562
249 cells under continuous ferrostatin-1 treatment. As before, the efficiency and specificity of the
250 screens were assessed based on effective depletion of characterized core essential genes²⁴ as
251 well as the lack of depletion of negative control guides (250 nontargeting and 125 intergenic
252 sgRNAs) (**Figure S7**).

253
254 To our surprise, this screen did not identify any genes whose disruption significantly enhanced
255 K562 cold tolerance. By contrast, we identified 176 genes selectively required during cold
256 cycling relative to constant 37°C control conditions (FDR < 0.1, LFC < -0.1, and requiring >2
257 sgRNAs, **Figure 4b**). It is notable that K562 cold survival was sensitive to the targeting of larger
258 number of genes than the BHK-21 line, potentially indicating increased dependencies on
259 genetic pathways which are not essential in BHK-21 cells (**Figure S8, Table S6**). Among the
260 pathways identified, we honed in on the selenocysteine incorporation pathway and observed
261 *GPX4* and the selenocysteine incorporation genes *PSTK*, *SEPSECS*, and *EEFSEC* within the
262 top-ranked K562 cold-protective genes, suggesting that the GPX4 pathway confers significant
263 resistance to the cold not only in cold-tolerant hibernator cells, but also in cold-sensitive human
264 cells (**Figures 4c-g**). Notably, we identified 11 genes that were no longer essential (Fold
265 enrichment > 0.50, FDR < 0.10) in the presence of Ferrostatin-1, indicating that these genes act
266 to suppress cold-induced ferroptosis (**Figures 4h-n, Table S4, S5**). Although multiple pathways
267 have been described as suppressors of ferroptosis in other contexts³⁸⁻⁴², it is notable that 5 of
268 11 identified genes represent known components of the GPX4 pathway.

269
270 To confirm these findings, we generated three clonal *GPX4* knockout K562 cell lines and
271 confirmed the loss of GPX4 via immunoblotting (**Figure 5a**). Similar to our findings in BHK-21

272 cells, K562 *GPX4* knockout clones exhibited stunted growth and were expanded in the
273 presence of liproxstatin-1 (**Figure S4b**). Importantly, *GPX4* loss greatly increased cold-induced
274 cell death ($****P < 0.0001$) (**Figures 5a**), thus confirming an essential role for *GPX4* in human
275 cell cold tolerance. Similar effects were also observed upon acute pharmacologically inhibition
276 of *GPX4* with RSL3 or ML162 at 4°C ($****P < 0.0001$) (**Figures 5b, c**). These effects were
277 dependent on *GPX4* inhibition insofar as the cold tolerance of K562 *GPX4* knockout cells was
278 unaffected by RSL3 treatment (**Figure S9**). In addition, RSL3-driven cold-induced cell death
279 was rescued by either ferrostatin-1 or DFO treatment, indicating that RSL3-induced cell loss
280 occurs via the ferroptosis pathway (**Figure 5d**). Increased cold-induced death in the *GPX4*
281 knockout K562 cell lines could be rescued upon lentiviral expression of either the cytosolic
282 human (hs) or hamster (ma) *GPX4*, but not GFP or catalytically dead *GPX4* variants (**Figure**
283 **5e**). Together, our genetic and pharmacological studies reveal that K562 cells, despite being
284 significantly less cold-tolerant than hamster BHK-21 cells, also rely on the *GPX4* pathway to
285 suppress cold-induced ferroptosis.

286

287 **GPX4 catalytic activity is limiting for K562 cell cold tolerance**

288 Given that the *GPX4* pathway is active during cold exposure and essential for cold survival in
289 both hamster BHK-21 and human K562 cells, it is somewhat surprising that these cell lines
290 exhibit markedly different cold tolerances. In this regard, it has previously been suggested⁵ that
291 upon cold exposure human cells, in contrast to hibernator-derived cells, rapidly deplete
292 intracellular glutathione, an essential co-factor for *GPX4* function, which could thus account for
293 their increased cold sensitivity. To test this idea, we supplemented K562 growth media with
294 either cell-permeable Glutathione reduced ethyl ester (GSH-MEE), N-acetyl-cysteine (NAC), or
295 L-Cystine, a glutathione precursor; however, these interventions failed to significantly increase
296 K562 cells' cold tolerance under our culture conditions (**Figure S10**). We therefore examined
297 the possibility that *GPX4* protein levels in K562 cells are limiting for their cold tolerance. To this
298 end, we generated K562 lines overexpressing either human or hamster *GPX4*. Both of these
299 overexpression lines exhibited strikingly improved cold tolerance compared to the wild-type
300 K562 parental line and a GFP-overexpressing control cell line ($****P < 0.0001$) (**Figure 5f**).
301 Indeed, *GPX4*-overexpressing K562 cells displayed comparable cold tolerance to that of
302 hibernator-derived BHK-21 cells (**Figure 1d, g**). To confirm that increased *GPX4* catalytic
303 activity was responsible for the improved cell cold tolerance, we generated additional K562 lines
304 overexpressing catalytically dead forms of hamster or human *GPX4* in which the active site
305 selenocysteine was mutated to serine and found that these *GPX4* mutant lines exhibited no

306 increase in cold tolerance (**Figure 5f**). Taken together, these results strongly suggest that GPX4
307 abundance serve as a key limiting determinant of K562 cell cold tolerance. Moreover, our
308 finding that human and hamster GPX4 overexpression confer comparable increases in K562
309 cold tolerance may indicate that the intrinsic activity of the hamster and human GPX4 enzymes
310 are similar.

311

312 **GPX4 activity is broadly required for cold tolerance in primary cells across evolutionarily** 313 **distant mammalian species**

314 Given that our studies had largely employed a small number of transformed cell lines, we
315 sought to extend our investigation to examine cold tolerance in primary cell types as well as
316 cells derived from additional hibernating species. To this end, we obtained primary and
317 immortalized fibroblasts from human, mouse, and rat as well as from Syrian hamster, 13-lined
318 ground squirrel (*Ictidomys tridecemlineatus*), and horseshoe bat (*Rhinolophus ferrumequinum*),
319 three distantly related mammalian hibernators, and characterized their cold tolerance. While
320 hibernator-derived fibroblasts exhibited robust, roughly uniform cold tolerance, we observed a
321 surprisingly variable degree of cold tolerance across non-hibernator primary cells (**Figure 6a**),
322 with human dermal fibroblasts exhibiting a remarkable $79 \pm 4.93\%$ cell viability after seven days
323 at 4°C, comparable to that observed with hamster-derived BHK-21 cells.

324

325 To examine the role of GPX4 in primary cell cold resistance, we transduced cells with Cas9 and
326 sgRNAs targeting human *GPX4* to create a population of *GPX4* knockout human kidney
327 fibroblasts (**Figure 6b**). Consistent with our prior findings in cell lines, GPX4 loss resulted in
328 significantly decreased viability in the cold, which was largely rescued by ferrostatin-1 treatment
329 in fibroblast cells (**Figure 6b**). Indeed, RSL3 treatment significantly decreased the viability of
330 wild-type cold-exposed human kidney fibroblasts (**Figures 6c, d**), and these effects were
331 dependent on GPX4 inhibition as the cold tolerance of human kidney fibroblast *GPX4* knockout
332 cells was largely unaffected by RSL3 treatment (**Figure S4c**).

333

334 To more widely examine the dependence of primary cell cold tolerance on GPX4 activity, we
335 obtained and tested fibroblasts derived from six mammalian species. We found the GPX4
336 activity widely contributes to cold tolerance across hibernators and non-hibernators was
337 dependent on GPX4, as RSL3-treated cells showed increased cold-induced cell death that was
338 largely rescued by ferrostatin-1 treatment (**Figures 6e, f**). We also extended these findings to a
339 non-fibroblast cell type, obtaining similar results with primary cortical neuronal cultures prepared

340 from neonatal mice and hamsters (**Figures 6g, h**). Taken together, our data indicate that
341 primary cell types are strongly sensitive to GPX4 loss in the cold and suggest that their
342 differential cold sensitivities may reflect different levels of GPX4-mediated cold tolerance.

343

344 **Discussion**

345 Hibernators can lower their body temperature to ~4°C for several days to weeks, indicating that
346 their cells and tissues possess the ability to survive extended periods of cold. Previous studies
347 have indicated that ferroptosis contributes to cold-induced cell death in cultured human
348 cells^{5,8,37}; however, the genetic modifiers of cold sensitivity in hibernators and non-hibernators
349 have yet to be systematically explored. Here, we conducted a series of unbiased genome-wide
350 CRISPR-Cas9 screens in both hibernator- and non-hibernator-derived cells to investigate the
351 mechanisms controlling cellular cold tolerance. Our findings, further validated using stable
352 genetic knockout lines and pharmacological inhibitors, identify the GPX4 pathway as a critical
353 suppressor of cold-induced cell death. Indeed, overexpression studies in human K562 cells
354 suggest that GPX4 abundance can serve as a key limiting determinant of cellular cold tolerance.
355 Notably, Sone et al.⁴³ recently also identified GPX4 as a strong regulator of cold tolerance
356 through overexpression screening. These independent findings further support the current study
357 identifying GPX4 as a conserved suppressor of cold-induced cell death. The consistency of our
358 observations across diverse cell lines and primary cells, including cells derived from six different
359 mammalian species, argues that GPX4 serves as an essential and evolutionarily conserved
360 mechanism to protect cells from cold-induced ferroptotic cell death.

361

362 During the course of our studies, we made the surprising observation that cells stained with the
363 commonly employed membrane-impermeable dye trypan blue exhibit increased dye retention
364 immediately after cold exposure, an artifact not reflecting genuine cell death. Rather, cell
365 counting following brief rewarming yields more accurate results, in some cases reflecting
366 significantly higher cell viability than previously appreciated. Employing this modified approach
367 to measure cold-induced cell death across sixteen cell lines and primary cell types points to
368 more nuanced variations in cold survival across cell types. These differences are highlighted by
369 the pronounced contrast between the poor cold viability of human HT1080 cells and the robust
370 cold tolerance observed in human fibroblasts. The underlying basis of this transient cell
371 permeability for trypan blue following cold exposure remains unclear; however, it is noteworthy
372 that in *S. cerevisiae* heat and chemical insults have been found to induce a brief window of
373 membrane permeability to PI prior to membrane repair⁴⁴. Likewise, uptake of propidium ions

374 across intact cell membranes has been previously observed in bacteria showing high
375 membrane potentials⁴⁵. Our observations suggest that further investigation into the mechanisms
376 underlying transient membrane permeability in different cell types and stress conditions could
377 lead to improved methods for accurately measuring cell viability, ultimately enhancing our
378 understanding of cellular stress.

379

380 We report, to our knowledge, the first genome-scale hibernator CRISPR-Cas9 screen in cells
381 derived from Syrian hamster. To create a genome-scale CRISPR-Cas9 library, we implemented
382 a CRISPOR-based computational pipeline for sgRNA selection and benchmarked its success
383 by carrying out the hamster and human screens described here. Our validated sgRNA libraries
384 and associated algorithms should serve as a valuable resource to the hibernation community,
385 as well as other scientific communities developing CRISPR-based tools for non-model
386 organisms.

387

388 While our data point to GPX4 levels as a major determinant of cellular cold tolerance, whether
389 endogenous levels of functional Gpx4 across various cell types correlates with their cold
390 tolerance remains to be tested. It also remains possible that other factors such as GPX4
391 subcellular localization, the abundance of the cellular selenocysteine incorporation machinery,
392 the abundance of glutathione, as well as GPX4-pathway independent factors all play important
393 roles in limiting cold tolerance across various cell types. Although we did not see an increase in
394 cold cell viability upon treatment of K562 cells with GSH-MEE, it is notable that in our screens,
395 sgRNAs targeting genes involved in the glutathione biosynthesis (e.g. *GCLC*, *GSS*^{46,47}) showed
396 increased depletion in cold-exposed K562 versus BHK-21 cells (**Figure S10**, **Figure S11**). This
397 suggest a reduced dependency on the conventional glutathione biosynthetic pathway in cold-
398 exposed BHK-21 cells. In addition, while our data points to a key cellular need to reduce cold-
399 associated lipid hydroperoxides, the mechanisms that drive peroxide accumulation in the cold
400 remain unclear. Specifically, the roles of reactive oxygen species (ROS) production,
401 polyunsaturated fatty acid (PUFA) levels, and free iron concentration should be further explored
402 to understand the specific drivers of cold-induced ferroptotic cell death. Such insights have the
403 potential to inform the development of more effective strategies for managing conditions
404 exacerbated by cold exposure, such as ischemic injuries and organ transplantation.

405

406 We limited our current investigations to cell culture paradigms. However, future *in vivo* studies in
407 hibernating organisms that naturally undergo profound drops in core body temperature could

408 yield further insight into the adaptive mechanisms that govern cellular survival during periods of
409 hibernation and torpor, while also allowing for the study of cold tolerance mechanisms in cell
410 types that cannot presently be maintained in culture. Similarly, a *Gpx4* conditional knockout
411 mouse line has been generated and used to show that *Gpx4* is essential for mitochondrial
412 integrity and neuronal survival in adult animals⁴⁸; however, these animals have not yet been
413 used to evaluate the contribution of *Gpx4* to *in vivo* cellular and tissue cold tolerance.

414
415 The ability to hibernate and survive long-term cold exposure is present in many mammalian
416 species from rodents to bats to primates, raising the possibility that the ability to enter
417 hibernation and tolerate cold was an ancestral trait present in protoendotherms. Our observation
418 that a single pathway centered around GPX4 is required across diverse mammalian species to
419 protect cells from cold-induced cell death, raises a question whether GPX4 has a role in
420 protection from cold-induced ferroptosis in other cold-tolerant vertebrates including fish,
421 amphibians, reptiles, and birds that also enter torpor. Such studies will advance our
422 understanding of the evolved mechanisms by which cells mitigate cold-associated damage—
423 one of the most common challenges faced by cells and organisms in nature.

424

425 **Acknowledgments**

426 We thank Wei Li for generously sharing 13-lined ground squirrel (*Ictidomys tridecemlineatus*)
427 fibroblasts and Thomas P. Zwaka for sharing greater horseshoe bat (*Rhinolophus*
428 *ferrumequinum*) fibroblasts. We thank Amanda Chilaka and Sumeet Gupta of the Whitehead
429 Institute Genome Technology Core for high-throughput sequencing. We thank Aurora Lavin-
430 Peter, Aleksandar Markovski, Tara Thakurta, William S. Owens, Sheamin Khyeam, Karina
431 Smolyar, and Elena Assad for their technical support. We thank Whitney Henry, Matthew
432 Vander Heiden, Alison Ringel, Morgan Sheng, Myriam Heiman, and members of the Hrvatin
433 laboratory for providing feedback on the study. Schematics created with BioRender.com. This
434 material is based upon work supported by the National Science Foundation Graduate Research
435 Fellowship under Grant No. 2141064 and The Paul and Daisy Soros Fellowship for New
436 Americans (PSM). Research reported in this publication was supported by The G. Harold and
437 Leila Y. Mathers Charitable Foundation and the NIDDK/NIH under Award Number
438 DP2DK136123. The content is solely the responsibility of the authors and does not necessarily
439 represent the official views of the National Institutes of Health.

440

441 **Author contributions**

442 B.L., K.M.K., and S.H. conceived and designed the study. B.L. and K.M.K. designed, performed,
443 and analyzed experiments. B.L., K.M.K., H.R.K. designed and performed genome wide CRISPR
444 screens. A.K. assisted with the genome wide CRISPR screens. B.L. performed the genetic and
445 pharmacological studies to validate the screens. K.M.K. performed the experiments with primary
446 cells. E.M.F. and G.W.B. designed algorithms to select genome-wide Syrian hamster
447 (*Mesocricetus auratus*) CRISPR library. M.E.B. and P.B. immortalized mouse embryonic
448 fibroblasts and greater horseshoe bat (*Rhinolophus ferrumequinum*) fibroblasts. J.M.R., R.J.,
449 J.S.W., and E.C.G. advised on the study. B.L., S.H., and E.C.G led the writing of the manuscript
450 with contributions from other authors. E.C.G. and S.H. obtained funding for the research. All
451 authors approved and reviewed the manuscript.

452

453 **Declaration of interests**

454 The authors declare no competing interests.

455

456

457

458

459

460

461

462

463

464

465

466

467

468

469

470

471

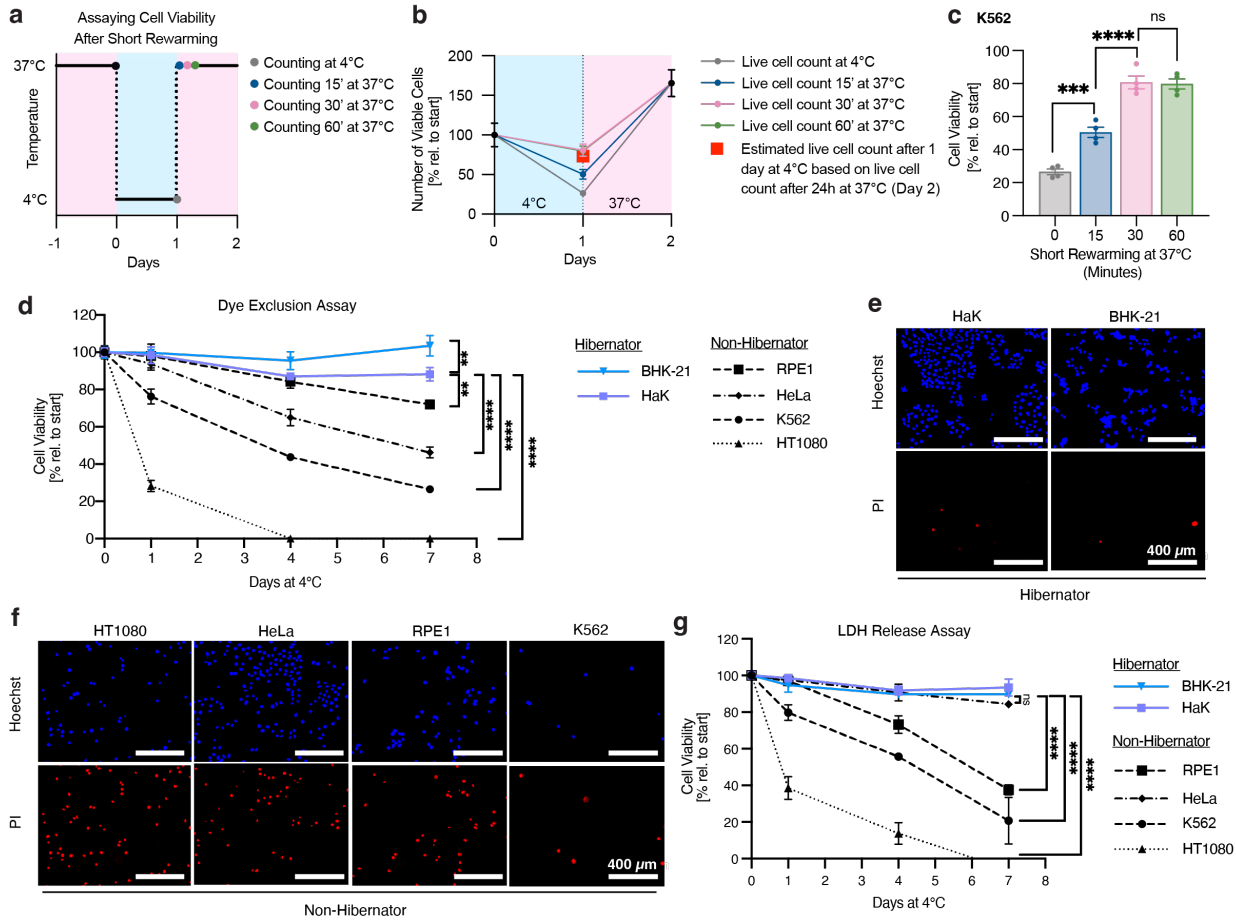
472

473

474

475

476 **Figures**



477

478 **Figure 1. Hibernator-derived cells exhibit increased cold resistance**

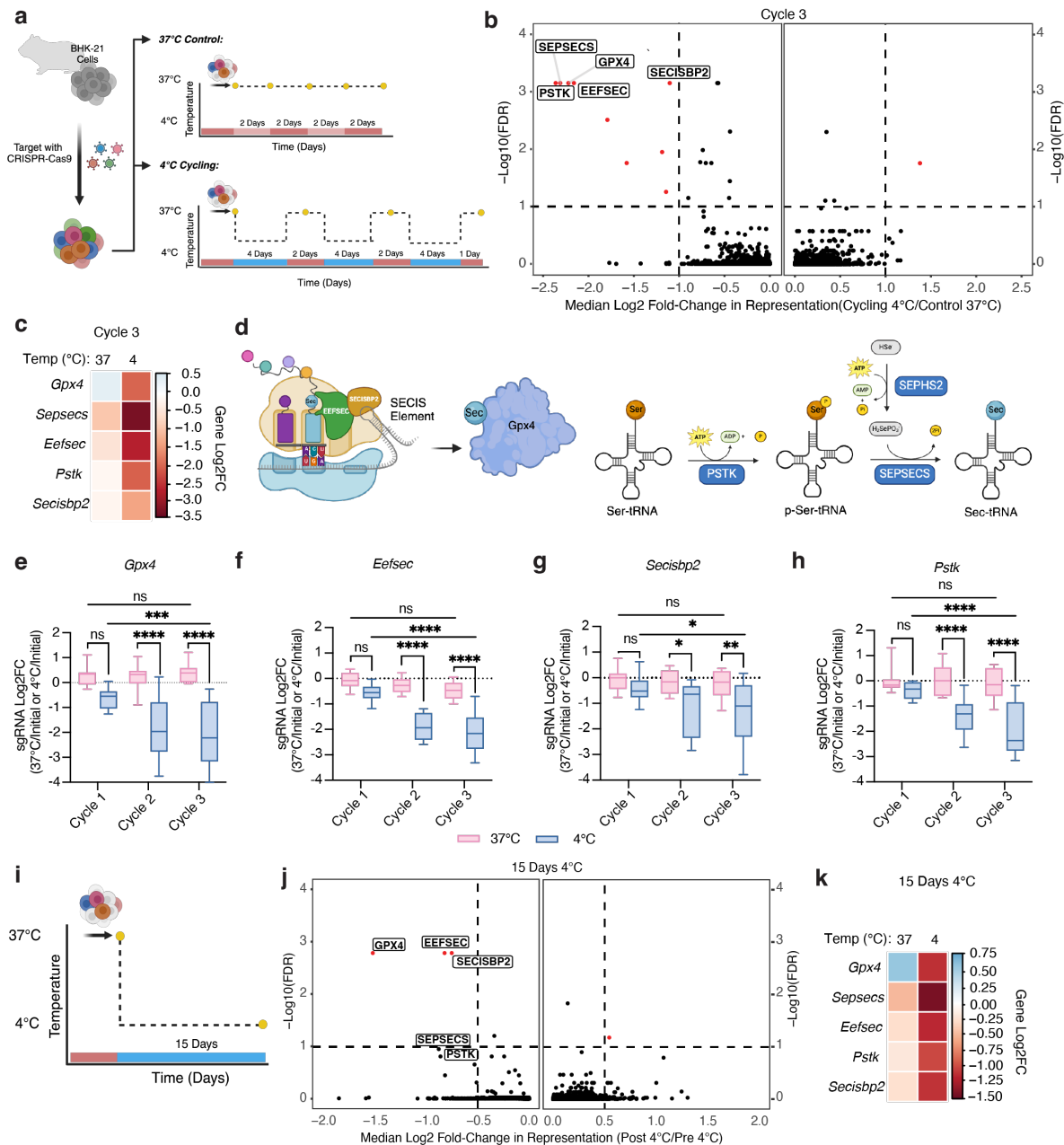
479 **a**, Schematic of cold cell viability counting, consisting of 1 day cold exposure (4°C), followed by
 480 a short rewarming at 37°C for 15, 30, or 60 minutes before trypan blue staining. **b**, Number of
 481 viable K562 cells based on trypan blue staining after one day at 4°C and subsequent rewarming
 482 for 24 hours at 37°C. Numbers are normalized to initial cell counts. Blue shaded regions indicate
 483 4°C exposure and shaded pink regions indicate 37°C exposure. Red square indicates
 484 calculated cell counts after one day at 4°C based on the viable cell number measured after 24
 485 hour rewarming. **c**, Viability of K562 cells was assessed by trypan blue staining after incubation
 486 at 37°C for 0, 15, 30, or 60 minutes following 24 hours at 4°C ($n = 4$). Cells incubated at 37°C
 487 for 15, 30, and 60 minutes show a significant increase in cell counts compared to cells counted
 488 without rewarming ($n = 4$ samples per condition, *** $P = 0.0007$, **** $P < 0.0001$). **d**, Viability of
 489 hibernator (BHK-21, HaK)- and non-hibernator (HeLa, RPE1, HT1080, K562)-derived cell lines
 490 at 4°C as measured by trypan blue staining. Hibernator-derived lines show significantly
 491 increased cold resistance compared to lines derived from non-hibernators at 7 days 4°C ($n = 4$

492 samples per data point, **** $P < 0.0001$). **e, f**, Fluorescence images of hibernator- and non-
493 hibernator-derived cell lines after 4 days at 4°C. Cultures were stained with 1 µg/mL Hoechst
494 33342 and 1 µg/mL propidium iodide (PI) to distinguish live and dead cells. **g**, Viability of
495 hibernator- and non-hibernator-derived cell lines at 4°C as measured by LDH release ($n = 4$
496 samples per data point, **** $P < 0.0001$). All values show mean \pm SEM, with significance
497 measured by one-way ANOVA adjusted for multiple comparisons by Dunnett's test. * $P < 0.05$;
498 ** $P < 0.01$; *** $P < 0.001$; **** $P < 0.0001$; ns $P > 0.05$.

499

500

501



502

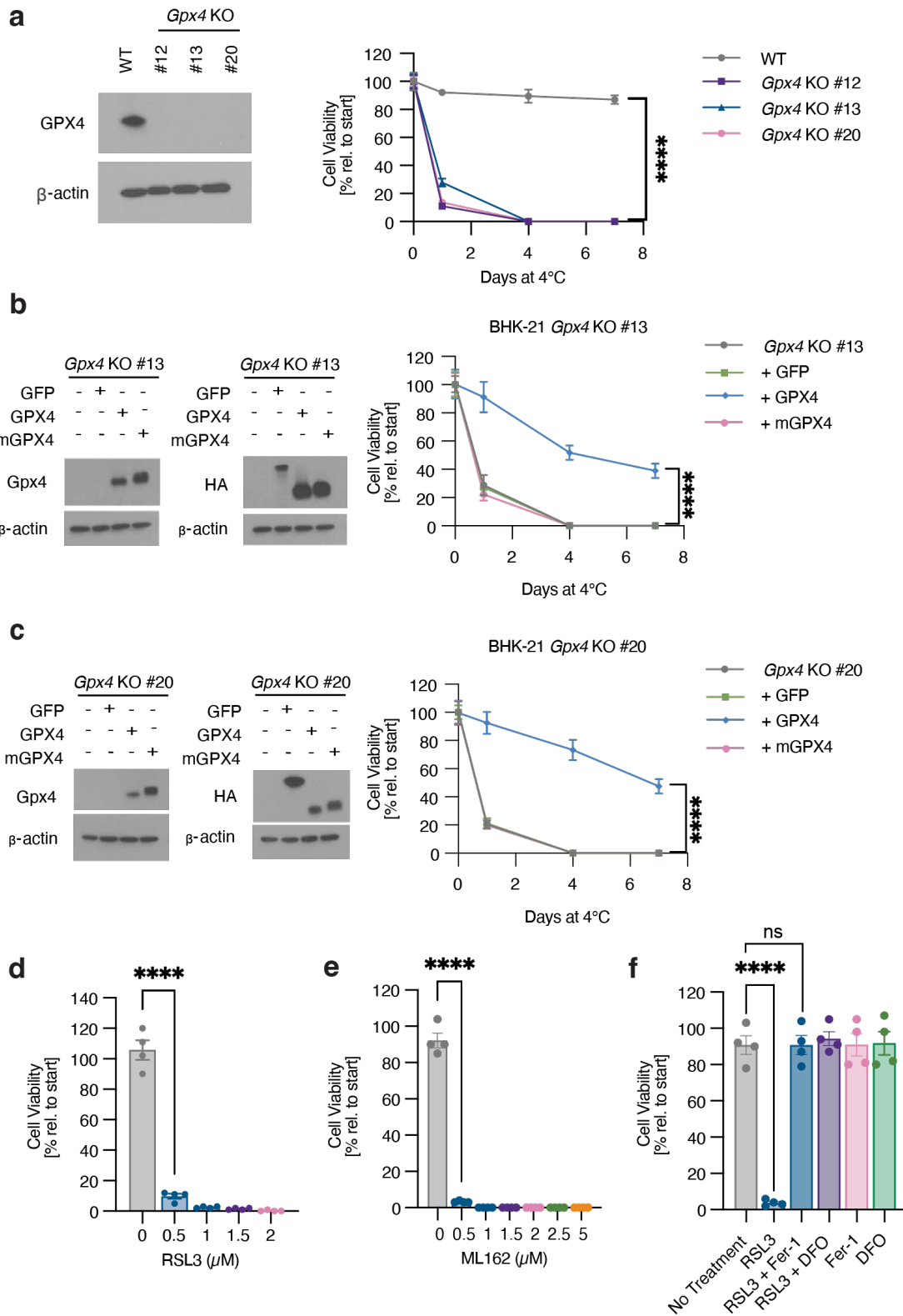
503 **Figure 2. Unbiased CRISPR screens identify the GPX4 pathway as necessary for cold-**
 504 **induced survival in hibernator-derived BHK-21 cells**

505 **a**, Schematic of CRISPR screen paradigm, consisting of four passages of control cells kept at
 506 37°C and three cycles of cold exposure (4°C) for 4 days followed by rewarming (37°C) for 2
 507 days. Yellow dots indicate points of sample collection. **b**, Volcano plot showing median log₂
 508 fold-change of genes after three cycles of cold exposure and rewarming (4°C) compared to cells
 509 following three passages at 37°C. Red dots indicate selectively required genes with a median
 510 log₂ fold-change < -1 or > 1 and FDR < 0.1. **c**, Heatmap of the median log₂FC of ferroptosis-

511 related genes after three cycles of cold exposure and rewarming (4°C) compared to three
512 passages at 37°C. **d**, Partial schematic of the selenocysteine incorporation pathway. Left:
513 Production of the GPX4 selenoprotein requires recoding of a UGA codon to the amino acid
514 selenocysteine (Sec). This process involves a cis-acting SECIS element within the *Gpx4* mRNA
515 3' UTR, SECIS binding protein 2 (SECISBP2), a specific eukaryotic elongation factor
516 (EEFSEC), and Sec-charged tRNA. Right: The Sec-charged tRNA is generated by the
517 combined action of Phosphoseryl-tRNA kinase (PSTK), Selenophosphate synthetase 2
518 (SEPHS2), and selenocysteine synthase (SEPSECS). **e-h**, Median log₂ fold-change (log₂FC) of
519 10 guides per targeted gene, showing guide depletion over three cycles of cold exposure and
520 rewarming. Significance between Cycle 1 versus Cycle 3 is measured by two-way ANOVA
521 adjusted for multiple comparisons by Dunnett's test. Significance between 37°C and 4°C for
522 each cycle is measured by two-way ANOVA adjusted for multiple comparisons by Bonferroni's
523 test. **e**, *Gpx4*, **f**, *Eefsec*, **g**, *Secisbp2*, **h**, *Pstk*. **i**, Schematic of CRISPR screen paradigm,
524 showing cells exposed to 4°C continuously for 15 days. Yellow dot indicates point of sample
525 collection. **j**, Volcano plot showing median log₂ fold-change in abundance of guides targeting
526 the indicated genes after 15 days of 4°C exposure compared to one passage at 37°C. Red dots
527 indicate selectively required genes with a median log₂ fold-change < -0.5 or > 0.5 and FDR <
528 0.10. **k**, Heatmap of the median log₂FC in abundance of guides targeting ferroptosis-related
529 genes after 15 days of 4°C exposure compared to 37°C control cultures. **P* < 0.05; ***P* < 0.01;
530 ****P* < 0.001; *****P* < 0.0001; ns *P* > 0.05.

531

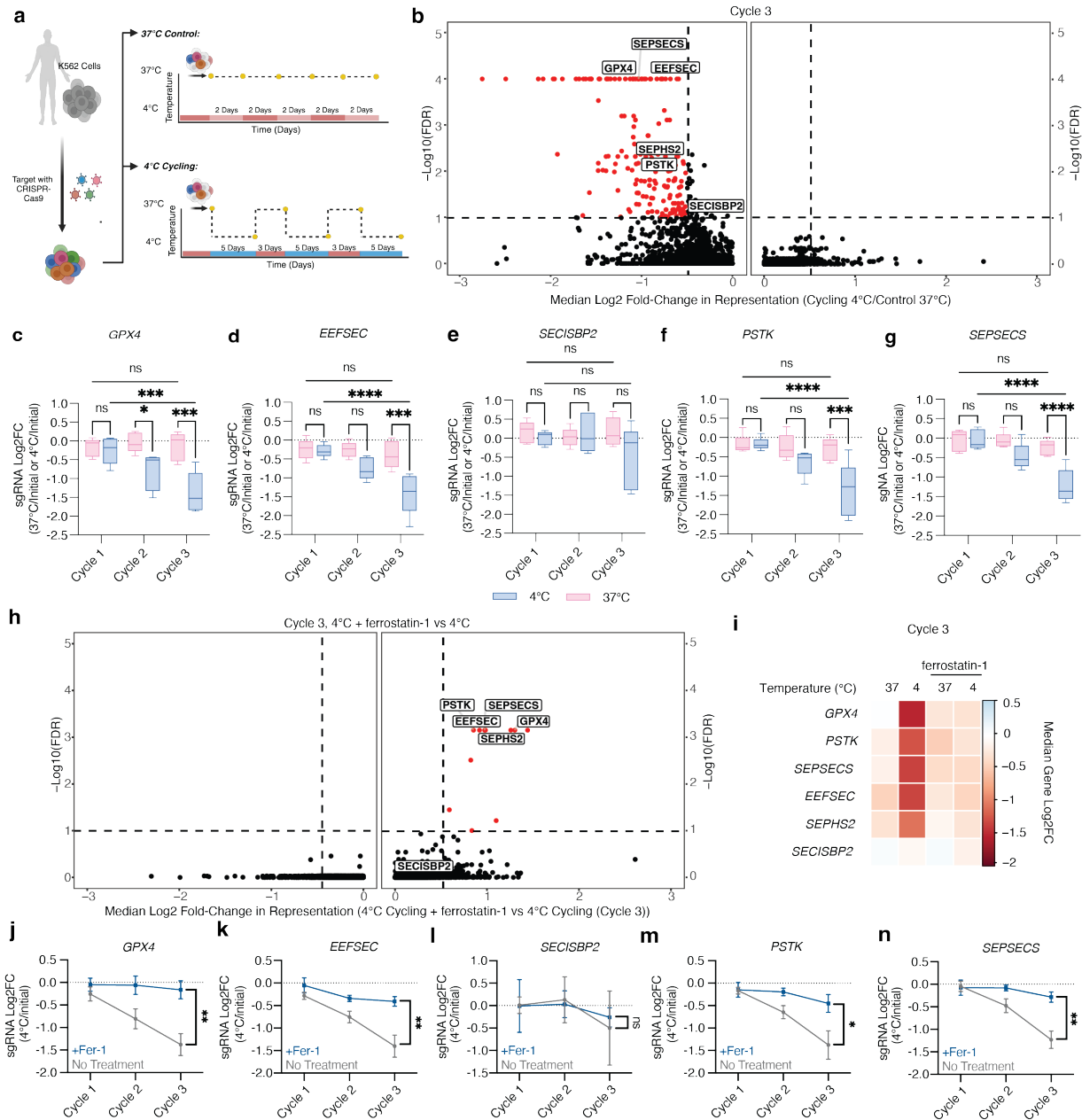
532



533

534 **Figure 3. GPX4 activity is required for BHK-21 cell cold tolerance**

535 **a**, Stable *Gpx4* knockout (KO) BHK-21 cell lines exhibit reduced cold tolerance. Left: Western
536 blot of wild-type (WT) and individual *Gpx4* KO clone lysates for GPX4 and β -actin loading
537 control. Right: Viability of *Gpx4* KO lines is significantly lower than WT BHK-21 cells at 7 days
538 4°C by trypan blue staining ($n = 4$, **** $P < 0.0001$), with complete cell death by four days at 4°C.
539 **b, c**, Reintroduction of wild-type Syrian hamster GPX4 (GPX4), but not a catalytically dead form
540 of GPX4 (mGPX4) rescues cold-induced cell death in two independent BHK-21 *Gpx4* KO clonal
541 cell lines. Left panels: Western blots for HA and GPX4 along with β -actin loading control. Right
542 panels: Expression of WT hamster GPX4 showed significantly higher cell viability at 7 days 4°C
543 compared to the corresponding parental *Gpx4* KO, GFP-, and mGPX4-expressing lines by
544 trypan blue staining ($n = 4$, **** $P < 0.0001$). **d, e**, Treatment with the GPX4 inhibitors RSL3 (**d**)
545 or ML162 (**e**) results in enhanced cold-induced death in BHK-21 cells by 4 days at 4°C as
546 measured by trypan blue exclusion ($n = 4$, **** $P < 0.0001$). **f**, Cold-induced BHK-21 cell death
547 upon RSL3 treatment occurs via ferroptosis. BHK-21 cells were placed at 4°C and treated with
548 RSL3 (1 μ M) and/or the ferroptosis inhibitor ferrostatin-1 (Fer-1, 1 μ M) or iron chelator DFO
549 (100 μ M) for 4 days ($n = 4$). Treatment with RSL3 resulted in significantly lower cell viability than
550 no treatment as determined by one-way ANOVA adjusted for multiple comparisons by Tukey's
551 HSD (**** $P < 0.0001$). All values show mean \pm SEM, with significance measured by two-tailed t
552 test, unless otherwise indicated. * $P < 0.05$; ** $P < 0.01$; *** $P < 0.001$; **** $P < 0.0001$; ns $P >$
553 0.05.
554



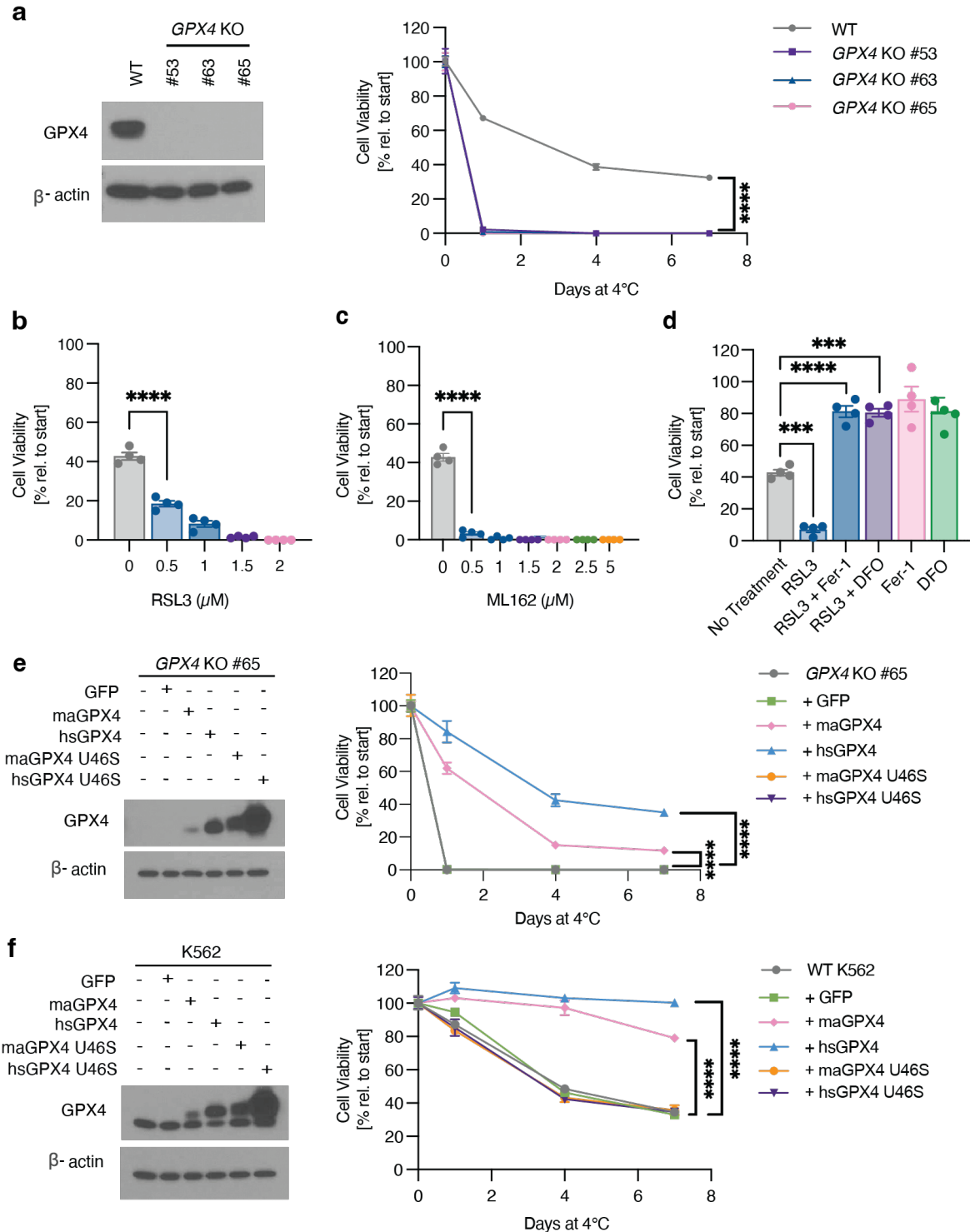
555

556

557 **Figure 4. Genome-wide CRISPR screens identify GPX4 as a suppressor of cold-induced**
 558 **cell death in human cells**

559 **a**, Schematic of CRISPR screen paradigm, consisting of three cycles of 5 days of cold exposure
 560 (4°C) interrupted by 3 day rewarming (37°C) periods. Yellow dots indicate points of sample
 561 collection. **b**, Volcano plot showing median log₂ fold-change in abundance of guides targeting
 562 the indicated genes after three cycles of 4°C cold exposure compared to three passages at
 563 37°C (Control). Red dots indicate selectively required genes with a median log₂ fold-change < -

564 0.5 or > 0.5 and FDR < 0.1. **c-g**, Combined median log₂ fold-change (log₂FC) of 5 sgRNAs per
565 targeted gene, showing sgRNA depletion over three cycles of cold exposure. Significance
566 between Cycle 1 versus Cycle 3 is measured by two-way ANOVA adjusted for multiple
567 comparisons by Dunnett's test. Significance between 37°C and 4°C for each cycle is measured
568 by two-way ANOVA adjusted for multiple comparisons by Bonferroni's test. **c**, *GPX4*, **d**,
569 *EEFSEC*, **e**, *SECISBP2*, **f**, *PSTK*, **g**, *SEPSECS*. **h**, Volcano plot showing median log₂ fold-
570 change in abundance of guides targeting the indicated genes after three cycles of 4°C cold
571 exposure in the presence or absence of 1 μM of ferrostatin-1. Red dots indicates selectively
572 required genes with a log₂ fold-change < -0.5 or > 0.5 and FDR < 0.1. **i**, Heatmap of the median
573 log₂FC in abundance of guides targeting ferroptosis-related genes after three cycles of cold
574 exposure (4°C) compared to 37°C control cultures with and without ferrostatin-1. **j-n**, Depletion
575 of 5 sgRNAs per gene over three cycles of cold exposure and rewarming with and without
576 ferrostatin-1 (1 uM) treatment. **j**, *GPX4* (***P* = 0.0047), **k**, *EEFSEC* (***P* = 0.0059), **l**, *SECISBP2*
577 (ns, *P* = 0.5457), **m**, *PSTK* (**P* = 0.0393), **n**, *SEPSECS* (***P* = 0.0029) as measured by two-
578 tailed t-test at Cycle 3. All values show mean ± SEM. **P* < 0.05; ***P* < 0.01; ****P* < 0.001; *****P*
579 < 0.0001; ns *P* > 0.05.
580
581



582

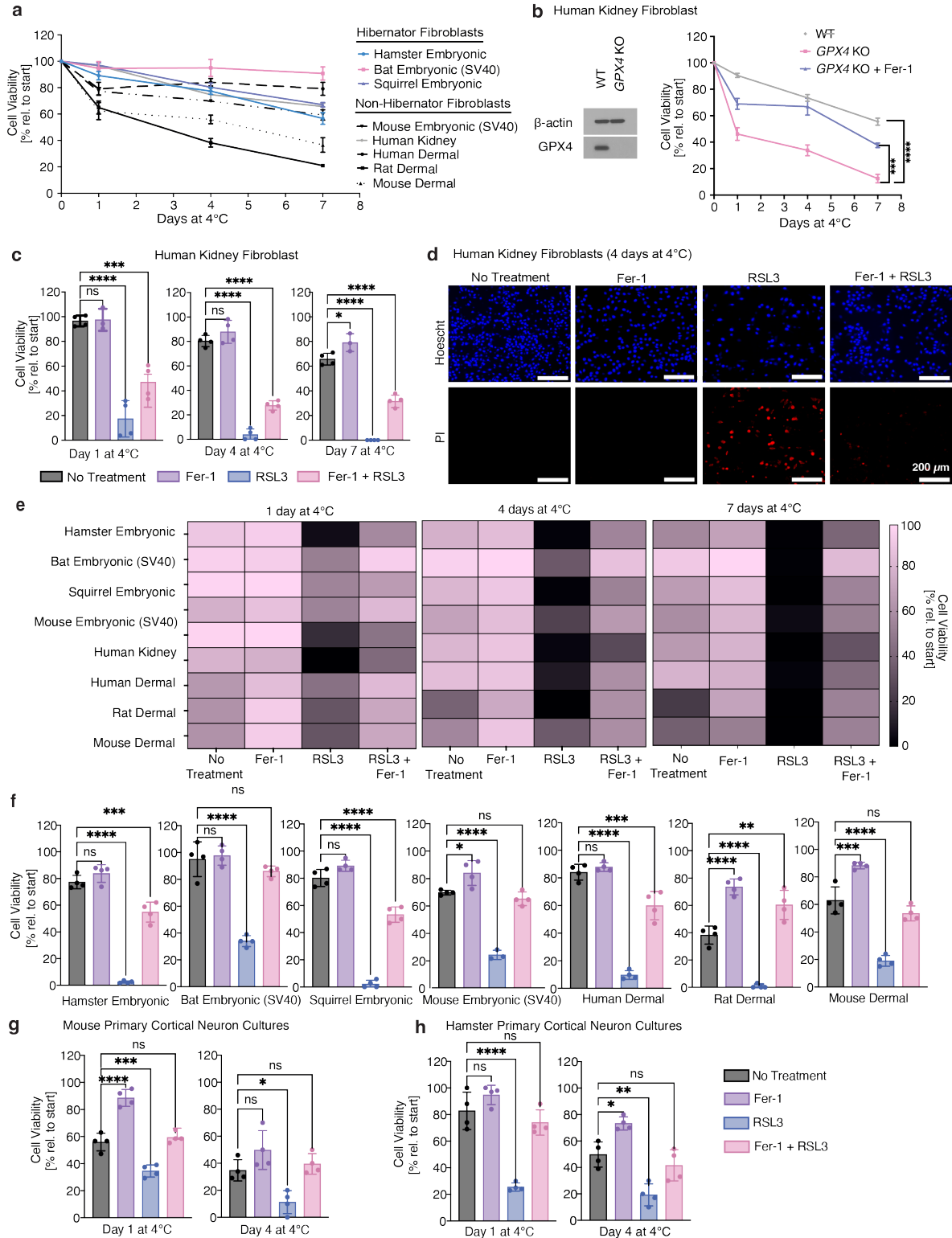
583 **Figure 5. Endogenous GPX4 activity is limiting for K562 cell cold tolerance**

584 a, Stable *GPX4* knockout (KO) K562 cell lines exhibit reduced cold tolerance. Left: Western

585 blotting of wild-type (WT) and individual *GPX4* KO clones for GPX4 and β-actin loading control.

586 Right: Viability of *GPX4* KO lines is significantly lower than WT K562 cells as measured by

587 trypan blue staining ($n = 4$, **** $P < 0.0001$), with complete cell death by one day at 4°C.
588 Significance measured by two-tail t-test at 7 days 4°C. **b, c**, Treatment with the GPX4 inhibitors
589 RSL3 (**b**) or ML162 (**c**) results in enhanced K562 cold-induced death by 4 days at 4°C ($n = 4$,
590 **** $P < 0.0001$) as measured by two-tailed t-test. **d**, Cold- and RSL3-induced K562 cell death
591 occurs via ferroptosis. K562 cells were placed at 4°C and treated with RSL3 (1 μM) and/or the
592 ferroptosis inhibitor ferrostatin-1 (Fer-1, 1 μM) or iron chelator DFO (5 μM) for 4 days ($n = 4$).
593 Treatment with RSL3 resulted in significantly lower cell viability than no treatment as determined
594 by one-way ANOVA adjusted for multiple comparisons by Tukey's HSD (** $P = 0.0002$). **e**,
595 Reintroduction of wild-type human (hs) or hamster (ma) GPX4, but not catalytically dead forms
596 of GPX4 (Gpx4 U46S), rescues cold-induced cell death in a K562 *GPX4* KO clonal cell line ($n =$
597 4). Left: Western blot for GPX4 levels and β-actin loading control. Right: Expression of WT
598 human GPX4 and hamster GPX4 resulted in significantly higher cell viability compared to the
599 corresponding parental *GPX4* KO, GFP-, and mutGPX4-expressing lines by trypan blue
600 staining, as measured by one-way ANOVA adjusted for multiple comparisons by Dunnett's test
601 at 7 days 4°C (**** $P < 0.0001$). **f**, Overexpression of wild-type human or hamster GPX4, but not
602 catalytically dead forms of GPX4 (mutGPX4), suppresses cold-induced cell death in a K562
603 cells ($n = 4$). Left: Western blot for GPX4, with β-actin loading control. Right: Expression of WT
604 human GPX4 and hamster GPX4 resulted in significantly higher cell viability compared to wild-
605 type, GFP-, and mutGPX4-expressing K562 lines by trypan blue staining, as measured by one-
606 way ANOVA adjusted for multiple comparisons by Dunnett's test at 7 days 4°C (**** $P < 0.0001$).
607 All values show mean ± SEM. * $P < 0.05$; ** $P < 0.01$; *** $P < 0.001$; **** $P < 0.0001$; ns $P > 0.05$.
608
609



610

611 **Figure 6. GPX4 is required for cold tolerance across both several hibernator and non-**
 612 **hibernator mammalian species and cell types**

613 **a**, Viability of hibernator cells (Syrian hamster embryonic fibroblasts, Greater horseshoe bat
614 embryonic fibroblasts, and 13-lined ground squirrel embryonic fibroblasts) and non-hibernator
615 cells (SV40-immortalized mouse embryonic fibroblasts, human adult kidney fibroblasts, human
616 adult dermal fibroblasts, rat adult dermal fibroblasts, and mouse adult dermal fibroblasts)
617 exposed to 4°C as measured by trypan blue staining ($n = 4$, **** $P < 0.0001$). **b**, Human kidney
618 fibroblast *GPX4* knockout cells exhibit reduced cold tolerance compared to WT cells. Left:
619 Western blot of wild-type (WT) and *GPX4* KO cells for GPX4 and β -actin loading control. Right:
620 Viability of *GPX4* KO cells is significantly lower than WT cells at 4°C as measured by trypan
621 blue staining ($n = 4$, **** $P < 0.0001$). **c**, Gpx4 activity is essential for cold survival of primary
622 human kidney fibroblasts. Human kidney fibroblasts were placed at 4°C and left untreated or
623 treated with RSL3 (1 μ M) and/or the ferroptosis inhibitor ferrostatin-1 (Fer-1, 1 μ M) for 7 days (n
624 = 4, **** $P < 0.0001$). **d**, Representative fluorescence images of human kidney fibroblasts after 4
625 days at 4°C with no treatment, 1 μ M Fer-1, 1 μ M RSL3, or 1 μ M Fer-1 and 1 μ M RSL3. Cultures
626 were stained with Hoechst 33342 and propidium iodide (PI) to identify live cells. **e**, Gpx4 activity
627 is essential for cold survival in hibernator cells (Syrian hamster embryonic fibroblasts, Greater
628 horseshoe bat embryonic fibroblasts, and 13-lined ground squirrel embryonic fibroblasts) and
629 non-hibernator cells (SV40-immortalized mouse embryonic fibroblasts, human adult kidney
630 fibroblasts, human adult dermal fibroblasts, rat adult dermal fibroblasts, and mouse adult dermal
631 fibroblasts). Cells were placed at 4°C and left untreated, treated with RSL3 (1 μ M), and/or
632 ferrostatin-1 (Fer-1, 1 μ M) for 7 days ($n = 4$). **f**, Expanded Day 4 data from **e**) indicates that
633 Gpx4 activity is essential for fibroblast survival in the cold across several hibernator and non-
634 hibernator species. Cells were placed at 4°C and left untreated or treated with RSL3 (1 μ M)
635 and/or ferrostatin-1 (Fer-1, 1 μ M) for 7 days ($n = 4$, **** $P < 0.0001$). **g-h**, Gpx4 activity is
636 essential in **g**) mouse primary cortical neuron cultures and **h**) hamster primary cortical neuron
637 cultures. Cells were placed at 4°C and left untreated, treated with RSL3 (1 μ M) and/or the
638 ferroptosis inhibitor ferrostatin-1 (Fer-1, 1 μ M) for 1 or 4 days ($n = 4$). RSL3 treatment increased
639 cell death, which was rescued by ferrostatin-1. All values show mean \pm SEM, with significance
640 measured by one-way ANOVA adjusted for multiple comparisons with Tukey's HSD. * $P < 0.05$;
641 ** $P < 0.01$; *** $P < 0.001$; **** $P < 0.0001$; ns $P > 0.05$.

642

643

644

645

646

647 **Tables**

648 **Table S1. Significant genes from Cycle 3 of genome-wide BHK-21 screen (median log₂**
649 **fold-change < -1 or > 1 and FDR < 0.1)**

Gene	Median Log ₂ FC	FDR
Rps29	1.3794	0.017327
Dld	-1.7915	0.003094
Eefsec	-2.1607	0.000707
Gpx4	-2.2215	0.000707
Lias	-1.1881	0.011251
Lipt1	-1.1444	0.05562
Pstk	-2.3621	0.000707
Secisbp2	-1.1041	0.000707
Sepsecs	-2.3116	0.000707
Ybey	-1.5789	0.017492

650

651 **Table S3. Significant genes from 15 days 4°C of genome-wide BHK-21 screen (median**
652 **log₂ fold-change < -0.5 or > 0.5 and FDR < 0.1)**

Gene	Median Log ₂ FC	FDR
LOC101827392	0.5431	0.066832
Eefsec	-0.81913	0.00165
Gpx4	-1.5133	0.00165
Secisbp2	-0.74996	0.00165

653

654 **Table S4. Significant genes from Cycle 3, 4°C + ferrostatin-1 vs 4°C of genome-wide K562**
655 **screen (median log₂ fold-change < -0.5 or > 0.5 and FDR < 0.1)**

Gene	Median Log ₂ FC	FDR
UBA3	0.59092	0.035754
PSTK	0.85375	0.000707
GPX4	1.3025	0.000707
CMIP	0.83519	0.09946
OXSM	0.82371	0.003094
HSCB	1.0999	0.060891
FTH1	1.4415	0.000707
SEPHS2	0.98322	0.000707
EEFSEC	0.91866	0.000707
FDXR	1.2588	0.000707
SEPSECS	0.9745	0.000707

656

657

658

659

660 **Methods**

661 **Cell culture**

662 Two hibernator-derived (BHK-21, HaK) and four non-hibernator-derived (HT1080, RPE1, HeLa,
663 K562) cell lines were used. All cells were purchased from ATCC. K562 cells were cultured in
664 Roswell Park Memorial Institute (RPMI) 1640 Medium (Gibco #11875093) supplemented with
665 10% fetal bovine serum (GeminiBio #100-106) and 1% penicillin/streptomycin. The remaining
666 cells were cultured in Dulbecco's modified Eagle's medium (DMEM) (Thermo Fisher Scientific
667 #12430054) supplemented with 10% fetal bovine serum (GeminiBio #100-106) and 1%
668 penicillin/streptomycin (Thermo Fisher Scientific #15140122).

669

670 **Cell viability assay**

671 Cells were seeded on 24-well culture plates at 50,000 cells per well and allowed to adhere for
672 24 hours at 37°C. Cells were then placed at 4°C with 5% CO₂ for varying time periods (1, 4, or 7
673 days), with a 30-minute rewarming at 37°C before assessing cell viability via trypan blue (TB)
674 (Thermo Fisher Scientific #15250061) staining. To assess cell viability using the TB assay, cells
675 were washed with PBS (Thermo Fisher Scientific #10010023), trypsinized and centrifuged at
676 300 x g for 3 minutes. The resulting pellet was resuspended in media, TB was added to a final
677 concentration of 0.2%, and cells were manually counted using a hemocytometer.

678

679 **Cell death assay (LDH)**

680 The amount of LDH in the supernatant was measured using the LDH-Glo Cytotoxicity Assay
681 (Promega J2380) following the manufacturer's protocol. The samples were mixed with reagents
682 on microplates, and luminescence was measured after a 30-minute incubation at room
683 temperature. The maximum amount of LDH in each was measured by fully lysing replicate wells
684 with 2% Triton X-100 (Thermo Fisher Scientific #A16046.AE). Background LDH signal was
685 measured from media-only wells and subtracted from sample values before normalization to
686 fully lysed wells in order to determine the amount of cytotoxicity per sample.

687

688 **Compound sources**

689 ML162 (SML0521), RSL3 (SML2234), erastin (E7781), 2'2'-Bipyridyl (D216305), and
690 necrostatin-1 (N9037°C) were obtained from MilliporeSigma. Ferrostatin-1 (S7243), Liproxstatin-
691 1 (S7699), and z-VAD-FMK (S7023) were purchased from Selleck Chemicals LLC.
692 Deferoxamine mesylate (ab120727) was purchased from Abcam.

693

694 **Genome-wide library design**

695 sgRNAs targeting the hamster genome build GCF_017639785.1 (BCM_Maur_2.0) were
696 designed based on NCBI Refseq gene annotations. Protein-coding regions of all gene exons
697 were filtered to retain only the most constitutively expressed exons and extended 20 nt on each
698 end. These regions were provided as input for CRISPOR⁴⁹ to pick and score all potential
699 guides. For each gene, guides were filtered by potential problem flags and then ranked by an
700 overall score derived from its efficiency (the Doench16/Fusi score), a custom motif penalty, a
701 fractional frameshift (from the Lindel score and the fractional distance to the beginning of the
702 region), and its specificity (derived from the MIT specificity score). For each gene, after the
703 guide with the best score was chosen, subsequent guides were also penalized by a location
704 score, adding a penalty for presence in the same exon and proximity to previously selected
705 guides for the same gene. If more than ten potential guides were identified for a gene, the ten
706 with the highest scores were selected.

707
708 For the human genome-wide library, we obtained a list of protein-coding genes in human based
709 on Ensembl release 98. The top five sgRNAs were picked for protein-coding genes and
710 controls, for a total of 102223 sgRNAs. Human intergenic sgRNAs were chosen by first
711 subsetting the list of all designed intergenic-region-targeted sgRNAs by Rank = 1, then requiring
712 the sgRNAs to target only one genomic locus. This list of 465 sgRNAs was ranked by MIT
713 specificity score in descending order, and the top 449 sgRNAs were chosen.

714

715 **Library cloning**

716 For the hamster library, 214,116 unique protospacer sequences targeting ~21,000 unique gene
717 symbols (> 99% with 10 sgRNAs/gene symbol), along with 2,299 intergenic-targeting and 250
718 nontargeting sequences were synthesized as an oligonucleotide pool (Agilent Technologies).
719 Separately, for the human library, 98,077 unique protospacer sequences targeting ~19,600
720 Ensembl transcript IDs (> 99.9% with 5 sgRNAs/gene), 449 intergenic-targeting sequences, 50
721 non-targeting sequences, and one sequence targeting the *AAVS1* safe harbor locus were
722 synthesized as an oligonucleotide pool (Agilent Technologies). A guanine nucleotide was
723 prepended to each 20-nucleotide protospacer sequence that began with A, C, or T. For both
724 hamster and human libraries, homology arms were prepended (5'-
725 TATCTTGTGGAAAGGACGAAACACC-3') and appended (5'-
726 GTTTAAGAGCTATGCTGGAAACAGCATAGC-3'). Additional adapters were pre- and appended
727 to the hamster library to enable subpool amplification if desired (subpool 1: 5'-
728 TCGGTGTATTGCTAGTGC GAACCCA-3' and 5'-ATCGTGTGAAAGGTGCCGCTATTGC-3';
729 subpool 2: 5'-GGTTCGTTCTACACATGGAAGCGGC-3' and 5'-
730 GAGGACTTCGAGTAGAACGCTGGCG-3'). Oligonucleotide pools were PCR amplified (forward

731 primer: 5'-TTTCTTGGCTTTATATATCTTGTGGAAAGGACGAAACACC-3'; reverse primer: 5'-
732 ATTTAAACTTGCTATGCTGTTTCCAGCATAGCTCTTAAAC-3') and cloned into
733 pLentiCRISPRv2-Opti (a gift from David Sabatini; Addgene plasmid # 163126;
734 <http://n2t.net/addgene:163126>; RRID:Addgene_163126). Briefly, 0.25 μ L of a 100 nM pool was
735 PCR amplified in 50 μ L reactions using Q5 HotStart DNA Polymerase (New England Biolabs)
736 for 10 cycles under the following conditions:

737

738	1 cycle	98 °C	2 minutes
739	10 cycles	98 °C	10 seconds
740		55-62 °C	15 seconds
741		72 °C	15 seconds
742	1 cycle	72 °C	2 minutes
743	1 cycle	4 °C	hold

744

745 All concentration steps were performed using a DNA Clean and Concentrator-5 kit
746 (ZymoResearch). Amplification from 8 gradient annealing reactions (55-62 °C) was assessed,
747 and successful reactions were pooled and concentrated. The vector was digested overnight at
748 37 °C with FastDigest Esp3I and FastAP (ThermoFisher Scientific), gel purified using a
749 Zymoclean gel DNA recovery kit (ZymoResearch), and concentrated. NEBuilder HiFi DNA
750 Assembly Master Mix (New England Biolabs) was used in 2 x 40-80 μ L bulk assembly
751 reactions, for a combined total reaction volume of 160 μ L containing 4 μ g of vector and 160 ng
752 of PCR amplicon (hamster) or 120 μ L total containing 3 μ g of vector and 120 ng of PCR
753 amplicon (human). Each bulk reaction was distributed in 5 μ L aliquots and incubated for 10
754 minutes at 52.2 °C, pooled, concentrated, introduced into Endura Electrocompetent DUO cells
755 (Lucigen) by electroporation, and plated on 8-16 LB agar with 75 μ g/mL carbenicillin in 245 mm
756 x 245 mm square bioassay dishes. A dilution series was also plated to assess electroporation
757 efficiency. Cells were incubated overnight at 30 °C, collected, and DNA was isolated using a
758 ZymoPURE II Plasmid DNA Maxiprep kit (ZymoResearch). Plasmid from separate
759 electroporations was combined proportionally based on electroporation efficiency for a
760 combined total library coverage of > 50-fold for each library. Sequence representation in the
761 libraries was assessed as described below.

762

763 **Lentivirus production for CRISPR-Cas9 screen**

764 For large-scale virus production, HEK-293T (1.5×10^7) cells were seeded in T175 cm² flasks in
765 DMEM (Thermo Fisher Scientific #12430054) supplemented with 10% fetal bovine serum
766 (GeminiBio #100-106). Media was changed 24 hours later to 20 mL viral production medium:
767 IMDM (Thermo Fisher Scientific #1244053) supplemented with 20% heat-inactivated fetal
768 bovine serum (GeminiBio #100-106). Cells were transfected 8 hours later with a mix containing
769 76.8 μ L Xtremegene-9 transfection reagent (MilliporeSigma #06365779001), 3.62 μ g pCMV-
770 VSV-G (Addgene plasmid # 8454; <http://n2t.net/addgene:8454>; RRID:Addgene_8454)⁵⁰, 8.28
771 μ g psPAX2 (a gift from Didier Trono; Addgene plasmid # 12260; <http://n2t.net/addgene:12260>;
772 RRID:Addgene_12260), and 20 μ g sgRNA/Cas9 plasmid and Opti-MEM (Thermo Fisher
773 Scientific #11058021) to a final volume of 1 mL. Media was changed 16 hours later to 55 mL
774 fresh viral production medium. Viral supernatant was collected and filtered through a 0.45 μ m
775 filter and aliquoted 48 hours post-transfection, then stored at -80°C until use.

776

777 **CRISPR screen in K562 cells**

778 K562 cells (3.9×10^8) were transduced with a pooled genome-wide lentiviral sgRNA library in a
779 Cas9-containing vector at MOI <1. The transduced cells were selected with 3 μ g/mL puromycin
780 (Thermo Fisher Scientific #A1113803), and 1×10^8 cells were passaged every 48-72 hours at a
781 density of 6×10^5 cells/T175 cm² flask in 45 mL RPMI 1640 (Gibco #11875093) medium
782 supplemented with 10% fetal bovine serum (GeminiBio #100-106) and 1%
783 penicillin/streptomycin for the duration of the screen. At 5 days post-puromycin selection, 1×10^8
784 cells were exposed to the cold with or without 1 μ M ferrostatin-1 (Selleck Chemicals #S7243).
785 K562 cells (1×10^8) were collected from the each of surviving populations after cold exposure
786 and/or rewarming as well as a matched untreated population. Genomic DNA was isolated using
787 the QIAmp DNA Blood Maxiprep kit (Qiagen # 51192), and high-throughput sequencing libraries
788 were prepared.

789

790 **CRISPR screen in BHK-21 cells**

791 BHK-21 cells (8.55×10^8) were transduced with a pooled genome-wide lentiviral sgRNA library in
792 a Cas9-containing vector at an MOI of 0.25. Transduced cells were selected with 2 μ g/mL
793 puromycin (Thermo Fisher Scientific #A1113803), and 2.56×10^8 cells were passaged every 48-
794 72 hours at a density of 5×10^6 cells/15-cm dish in DMEM (Thermo Fisher Scientific #12430054)
795 medium supplemented with 10% fetal bovine serum (GeminiBio #100-106) and 1%
796 penicillin/streptomycin for the duration of the screen. At 6 days post-puromycin selection,
797 2.56×10^8 cells were exposed to the cold. Cells (2.4×10^8) were collected from each of the

798 surviving populations after cold exposure and/or rewarming as well as from a matched
799 untreated population. During the cycles, cells were placed at 4°C for 4 days, then rewarmed to
800 37°C for 24 hours, reseeded, and after a further 24 hours at 37°C were placed back at 4°C to
801 begin a subsequent cycle. Genomic DNA was isolated using the QIAamp DNA Blood Maxiprep
802 kit (Qiagen # 51192), and high-throughput sequencing libraries were prepared.

803

804 **Sequencing library preparation**

805 The QIAamp DNA Blood Maxiprep Kit (Qiagen # 51192) was used to extract genomic DNA
806 (gDNA) from cell pellets of $2.5\text{-}5 \times 10^7$ cells according to manufacturer's instructions with minor
807 modifications: QIAGEN Protease was replaced with 500 μL of 10 mg/mL Proteinase K
808 (MilliporeSigma # 3115879001) in water, and cells were lysed overnight; centrifugation was
809 performed for 2 minutes and 5 minutes after the first and second wash, respectively; 1 mL of
810 water preheated to 70 °C was used to elute gDNA, followed by centrifugation for 5 minutes.
811 gDNA was quantified using the Qubit dsDNA HS Assay kit (Thermo Fisher Scientific #Q32851).
812 PCR amplification of sgRNA sequences was performed in 50 μL reactions using ExTaq
813 Polymerase (Takara Bio #RR001B) with the following program:

814

815	1 cycle	95 °C	5 minutes
816	16, 24, or 28 cycles	95 °C	10 seconds
817		60 °C	15 seconds
818		72 °C	45 seconds
819	1 cycle	72 °C	5 minutes
820	1 cycle	4 °C	hold

821

822 Using the following primers:

823 Forward: 5'- AATGATACGGCGACCACCGAGATCTACACCCCACTGACGGGCACCGGA - 3'

824 Reverse: 5'- CAAGCAGAAGACGGCATAACGAGATCnnnnnnTTTCTTGGGTAGTTTGCAGTTTT
825 - 3'

826 Where "nnnnnn" denotes the barcode used for demultiplexing.

827

828 Plasmid libraries were amplified for 16 cycles using 10 ng input per 50 μL reaction. gDNA was
829 initially amplified for 24 (human) or 28 (hamster) cycles in 50 μL test PCR reactions with 1, 3, 4,
830 5, or 6 μg input. An additional 20-75 reactions were performed using 3-6 μg per reaction
831 (sampling 150 μg or 300 μg gDNA total for human and hamster screens, respectively). Select-a-

832 Size DNA Clean and Concentrator (Zymo Research #D4080) or HighPrep PCR (MagBio
833 Genomics) was used to purify 95-100 μ L of each pooled sample, which were eluted with 12-20
834 μ L water and quantified using the Qubit dsDNA HS Assay kit prior to sequencing for 50 cycles
835 on an Illumina Hiseq 2500 or NovaSeq using the following primers:

836
837 Read 1 sequencing primer: 5'-
838 GTTGATAACGGACTAGCCTTATTTAACTTGCTATGCTGTTTCCAGCATAGCTCTTAAAC - 3'
839 Index sequencing primer: 5'-
840 TTTCAAGTTACGGTAAGCATATGATAGTCCATTTTAAAACATAATTTTAAAAGTCAAACACTAC
841 CCAAGAAA - 3'

842

843 **CRISPR screen data analysis**

844 Sequencing reads from the human screen were trimmed and mapped to the sgRNA library
845 using Bowtie version 1.0.0⁵¹, allowing no mismatches, and counted. Sequencing reads from the
846 hamster screen were trimmed and mapped to the sgRNA library using a combination of
847 command line prompts and a custom Python function which generated a dataframe of counts
848 which perfectly (no permissibility for any base mismatches) matched sequenced reads to the full
849 guide library (code supplied on Github). Data from both human and hamster screens was
850 similarly analyzed using MAGeCK version 0.5.9.5⁵² using a gene test false discovery rate (FDR)
851 threshold of 0.05, the FDR method for p-value adjustment, and the median as the gene-level
852 scoring metric.

853

854 PANTHER overrepresentation test was conducted on a set of 204 genes (FDR < 0.1) from the
855 third cycle of the human K562 CRISPR-Cas9 screen ['Analyzed List']. A list of genes expressed
856 in K562 cells at 37°C collected from bulk RNA sequencing was used as the ['Reference List']:
857 <https://pantherdb.org/tools/compareToRefList.jsp>. Fisher's Exact test type and false discovery
858 rate correction were utilized. Bulk RNA sequencing of K562 cells at 37°C was conducted by
859 generating a cDNA library prepared by depleting rRNA using the NEBNext rRNA Depletion Kit
860 (Human/Mouse/Rat) (New England Biolabs) and then the NEBNext Ultra II Directional RNA
861 Library Prep Kit (New England Biolabs). cDNA libraries were amplified using appropriate
862 multiplexed index primers for PCR.

863

864 Data was visualized using R version 4.2.1⁵³ corrplot package version 0.92⁵⁴ and base graphics,
865 and GraphPad Prism version 10.

866

867 **Generation of stable CRISPR/Cas9-targeted cell lines**

868 Homology arms were prepended (5'-TATCTTGTGGAAAGGACGAAACACC-3') and appended
869 (5'-GTTTAAGAGCTATGCTGGAAACAGCATAGC-3') to the top two ranked human or hamster
870 *GPX4*-targeting guides from the genome-wide screens. These guides were PCR amplified and
871 cloned into pLentiCRISPRv2-Opti (a gift from David Sabatini; Addgene plasmid # 163126;
872 <http://n2t.net/addgene:163126>; RRID:Addgene_163126). K562 and BHK-21 cells were then
873 infected with LentiCRISPRv2. Transduced cells were selected with 3 µg/mL puromycin (Thermo
874 Fisher Scientific #A1113803) for K562 cells and 2 µg/mL for BHK-21 cells beginning two days
875 after infection. After one passage, cells were sorted (BD FACSAria™ Fusion Flow Cytometer)
876 into 96-well plates, at one cell per well to generate clonal knockout cell lines. Cells were cultured
877 in media with 2.5 µM liproxstatin-1 (Selleck Chemicals #S7699) to prevent cell death. Western
878 blotting was used to confirm *GPX4* loss in individual knockout clones prior to further use.

879

880 Human sgRNA:

881 5'- CGTGTGCATCGTCACCAACG - 3'

882 5'- CTTGGCGGAAAACCTCGTGCA - 3'

883

884 Hamster sgRNA:

885 5'- CGTGTGCATCGTCACCAACG - 3'

886 5'- CTTGGCTGAGAATTCGTGCA - 3'

887

888 **Generation of CRISPR/Cas9-targeted human kidney fibroblast pooled cells**

889 Primary human kidney fibroblasts were infected with LentiCRISPRv2 with sgRNAs targeting
890 *GPX4*, using the top two ranked *GPX4*-targeting guides from the genome-wide human k562
891 screen. Transduced cells were selected with 1 µg/mL puromycin (Thermo Fisher Scientific
892 #A1113803) beginning four days after infection. Cells were cultured in media with 2.5 µM
893 liproxstatin-1 (Selleck Chemicals #S7699) to prevent cell death. Western blotting was used to
894 confirm *GPX4* loss in individual knockout clones prior to further use.

895

896 **Immuoblotting**

897 Cells were plated at 6×10^5 cells per well in a 6-well plate and maintained overnight at 37°C.

898 Cells were then collected when wells were confluent. The media was aspirated, and cells were
899 washed with ice-cold PBS (Thermo Fisher Scientific #10010023). Cells were scraped in 100 µL

900 of RIPA buffer (150 mM NaCl, 1% Triton X-100, 0.5% Na-Dexycholate, 0.1% SDS, 50 mM Tris,
901 pH 8) with protease inhibitors (MilliporeSigma #04693159001) and collected in microcentrifuge
902 tubes. The contents were then vortexed for 30 minutes at 4°C and centrifuged at 16000 x g for
903 20 minutes at 4°C. Protein content of the samples was measured using the Pierce BCA Protein
904 Assay kit (Thermo Fisher Scientific #23225) and resuspended in 100 µL of RIPA buffer with
905 protein loading dye (10% SDS, 500 mM DTT, 50% Glycerol, 250 mM Tris-HCl and 0.5%
906 bromophenol blue dye, pH 6.8). Protein samples were boiled for 5 minutes at 95°C, vortexed,
907 and centrifuged at 16000 x g for 5 minutes before loading onto a gel. The gel was run at 120 V
908 for 2 hours before being transferred to a Polyvinylidene difluoride (PVDF) membrane (Thermo
909 Fisher Scientific #88518). The transfer cassette was run at 45 V for 2 hours. The membranes
910 were then transferred to 5% milk TBST (1X Tris-Buffered Saline, 0.1% Tween® 20 Detergent)
911 and shaken for 15 minutes before being washed in TBST. Primary antibodies recognizing GPX4
912 (Abcam #ab41787) or HA (Cell Signaling Technology #3724) were added at 1:1000 in 5% BSA
913 (MilliporeSigma #A9418) and incubated overnight at 4°C. The membrane was then washed 3
914 times in 1x TBST and 1:3000 anti-rabbit secondary antibody (Cell Signaling Technology #7074)
915 in 5% milk TBST was added. Membranes were incubated for 1 hour at room temperature and
916 washed 3x in 1x TBST. Membranes were then incubated in Pierce™ ECL Western Blotting
917 Substrate (Thermo Fisher Scientific #32106) for 5 minutes before imaging.

918

919 **Generation of HA-GPX4 and HA-GFP overexpression constructs**

920 To generate GPX4-overexpression lines, entire human *GPX4* (cytosolic; NM_001367832.1) and
921 hamster *Gpx4* were amplified from the cDNA of K562 and BHK-21 cells, respectively. The
922 cloned transcript fragments include the 3' UTR that contains the SECIS element necessary for
923 selenocysteine incorporation. The *GPX4* genomic DNA fragments were cloned into pLJM1
924 (Addgene plasmid # 19319; <http://n2t.net/addgene:19319>; RRID:Addgene_19319) and
925 confirmed via sequencing. To create GPX4 mutants, (U46S), non-overlapping primers were
926 used to create mutations via inverse PCR, as previously described⁵⁵, converting the UGA stop
927 codon to UCA, encoding serine. GFP was amplified from pLJM1-EGFP (Addgene plasmid #
928 19319; <http://n2t.net/addgene:19319>; RRID:Addgene 19319) with Gibson overhangs to enable
929 insertion into a lentivirus vector. HA-GPX4 and HA-GFP DNA fragments were then amplified by
930 PCR and cloned into blasticidin lentiviral vectors [gift from Whitney Henry at the Whitehead
931 Institute for Biomedical Research] using standard cloning methods, with point mutations in the
932 PAM and guide sequences to prevent targeting of exogenously expressed *GPX4*.

933

934 HEK-293T cells (5×10^5) were seeded in 2 wells of a 6-well plate in DMEM (Thermo Fisher
935 Scientific #12430054) supplemented with 10% fetal bovine serum (GeminiBio #100-106).
936 Media was changed 16 hours later to 2 mL per well of viral production medium: IMDM (Thermo
937 Fisher Scientific #1244053) supplemented with 20% heat-inactivated fetal bovine serum
938 (GeminiBio #100-106). Cells were transfected 8 hours later with a mix containing 4.22 μ L
939 Xtremegene-9 transfection reagent (MilliporeSigma #06365779001), 181 ng pCMV-VSV-G
940 (Addgene plasmid # 8454; <http://n2t.net/addgene:8454>; RRID:Addgene_8454)⁵⁰, 414 ng
941 psPAX2 (a gift from Didier Trono; Addgene plasmid # 12260; <http://n2t.net/addgene:12260>;
942 RRID:Addgene_12260), and 1 μ g HA-GPX4 or HA-GFP plasmid and Opti-MEM (Thermo Fisher
943 Scientific #11058021) to a final volume of 50 μ L per well. Media was changed 16 hours later to
944 2.5 mL per well of fresh viral production medium. Viral supernatant was collected and aliquoted
945 48 hours post-transfection, then stored at -80°C until use.

946
947 K562 or BHK-21 cells (6×10^5 , wild-type and GPX4 knockout clones) were transduced with the
948 lentiviral HA-tagged GPX4 or GFP in the presence of 10 μ g/mL polybrene. After 8 hours of
949 incubation at 37°C , media was changed to virus-free media. After 48 hours, the transduced cells
950 were selected with blasticidin (Thermo Fisher Scientific #A1113903) at a concentration of 6
951 μ g/mL for K562 cells and 4 μ g/mL for BHK-21 cells. Overexpression of GPX4 and GFP was
952 confirmed via immunoblotting.

953

954 **Primary cell culture**

955 Three hibernator (13-lined ground squirrel postnatal dermal fibroblasts [gift from Wei Li at Duke
956 University], SV40-immortalized Greater horseshoe bat embryonic dermal fibroblasts [gift from
957 Rudolf Jaenisch at the Whitehead Institute for Biomedical Research], and Syrian golden
958 hamster embryonic primary dermal fibroblasts [isolated]) and five non-hibernator (mouse
959 embryonic SV40-immortalized dermal fibroblasts [gift from Jonathan Weissman at the
960 Whitehead Institute for Biomedical Research], adult human kidney fibroblasts [purchased from
961 ATCC], adult human dermal fibroblasts [purchased from ATCC], adult rat dermal fibroblasts
962 [purchased from ATCC], and adult mouse fibroblasts [purchased from ATCC]) primary cells
963 were cultured in Dulbecco's modified Eagle's medium (Thermo Fisher Scientific #12430054)
964 supplemented with 10% fetal bovine serum (GeminiBio #100-106) and 1%
965 penicillin/streptomycin (Thermo Fisher Scientific #15140122). Cells were seeded on 24-well
966 culture plates at $\sim 50,000$ cells per well and allowed to adhere for 24 hours at 37°C . Cells were
967 then placed at 4°C with 5% CO_2 for varying time periods (1, 4, or 7 days), with a 30-minute

968 rewarming at 37°C before assessing cell viability via trypan blue (TB) (Thermo Fisher Scientific
969 #15250061) staining. To assess cell viability using the TB assay, cells were washed with PBS
970 (Thermo Fisher Scientific #10010023), trypsinized and centrifuged at 300 x g for 3 minutes. The
971 resulting pellet was resuspended in media, TB was added to a final concentration of 0.2%, and
972 cells were manually counted using a hemocytometer.

973

974 **Primary neuron isolation and culture**

975 Primary Syrian golden hamster and C57BL/6 mouse cortical neurons were isolated at postnatal
976 day 0. The day before isolation, standard tissue culture treated plates were coated with 3 µg/mL
977 Poly-L-Ornithine (MilliporeSigma #P4957) and warmed at 37°C for 24 hours. The morning of
978 isolation, wells were washed with 1X PBS (Thermo Fisher Scientific #10010023). To isolate
979 neurons, pups were placed on ice for 2-5 minutes until movement ceased. Afterwards, they
980 were washed with 10% ethanol, decapitated, and their heads placed in a 10x dissociation media
981 bath (10.16 g MgCl₂ hexahydrate and 11.915 g HEPES in 450 mL HBSS brought to a pH of 7
982 using NaOH with subsequent addition of 1.182 g of kynurenic acid heated to 65% while stirring
983 until the solution was fully dissolved and cooled to room temperature and adjusted to a pH of
984 7.2. The dissociation media was then diluted from 10X to 1X in HBSS and filtered through a
985 0.22-µm vacuum filter). Dissected brains were placed in fresh dissociation media, where the
986 cortices were dissected out and transferred to 50 mL Falcon tubes on ice containing 1X
987 dissociation media. Afterwards, the dissociation media was removed from the cortices and
988 replaced with papain solution (5 mL 1x dissociation media, 5-7 grains of L-Cysteine, and 172 µL
989 Worthington papain [crystalline suspension in 50mM sodium acetate, pH 4.5 incubated in
990 1.1mM EDTA, 0.067mM mercaptoethanol and 5.5mM cysteine-HCl at 37°C. Activates to 20
991 units per 1 mg protein]) that was preheated to 37°C for 30 minutes. The cortices were incubated
992 in the papain solution for 3-5 minutes at 37°C. Afterwards, the papain solution was replaced with
993 trypsin inhibitor solution (10 mg of trypsin inhibitor dissolved in 10 mL of 1X dissociation media,
994 preheated to 37°C) and incubated subsequently at 37°C for 3-5 minutes, repeated 3 times.
995 Afterwards, the trypsin inhibitor solution was carefully removed and replaced with 6 mL of
996 preheated complete neurobasal media (5 mL of GlutaMAX5, 10 mL of B-27, 5 mL of
997 penicillin/streptomycin in neurobasal media filtered through a 0.22-µm vacuum filter). Using a 5
998 mL pipette tip, cortices were triturated until no tissue clumps were present. The cortices were
999 then passed through a 100-µm cell strainer to remove large debris and centrifuged at 300 x g for
1000 3 minutes before resuspension in 5 mL of complete neurobasal media before plating at a

1001 density of 50,000 mixed cortical neuron isolated cells per well of a 24 well plate. Subsequently,
1002 50% of the media was replaced every second day with fresh 37°C pre-warmed media.

1003

1004 **Statistical analyses and software information**

1005 Data are generally plotted as mean ± S.E.M. unless otherwise indicated. No statistical methods
1006 were used to predetermine sample sizes. Unless otherwise indicated, all replication numbers in
1007 the figure legends (n) indicate biological replicates. Statistical significance was determined using
1008 a two-tailed Student's T-test, one-way ANOVA, or two-way ANOVA using Prism 10 software
1009 (GraphPad Software) unless otherwise indicated. Statistical significance was set at $p \leq 0.05$
1010 unless otherwise indicated. Figures were finalized in Adobe Illustrator 2024.

1011

1012 **Supplemental information**

1013 Document S1. Figures S1-S11

1014 Table S2. Excel file containing hamster screen data, related to Figure 2

1015 Table S5. Excel file containing human screen data, related to Figure 4

1016 Table S6. Excel file containing GO_Biological Processes, related to Figure S8

1017

1018 **References**

- 1019 1. Cheshire, W.P. (2016). Thermoregulatory disorders and illness related to heat and cold
1020 stress. *Autonomic Neuroscience* 196, 91–104. <https://doi.org/10.1016/j.autneu.2016.01.001>.
- 1021 2. Physiology, Thermal Regulation - StatPearls - NCBI Bookshelf
1022 <https://www.ncbi.nlm.nih.gov/books/NBK499843/>.
- 1023 3. Tan, C.L., and Knight, Z.A. (2018). Regulation of body temperature by the nervous system.
1024 *Neuron* 98, 31–48. <https://doi.org/10.1016/j.neuron.2018.02.022>.
- 1025 4. Morrison, S.F., and Nakamura, K. (2019). Central Mechanisms for Thermoregulation. *Annu*
1026 *Rev Physiol* 81, 285–308. <https://doi.org/10.1146/annurev-physiol-020518-114546>.
- 1027 5. Hendriks, K.D.W., Joschko, C.P., Hoogstra-Berends, F., Heegsma, J., Faber, K.-N., and
1028 Henning, R.H. (2020). Hibernator-Derived Cells Show Superior Protection and Survival in
1029 Hypothermia Compared to Non-Hibernator Cells. *IJMS* 21, 1864.
1030 <https://doi.org/10.3390/ijms21051864>.
- 1031 6. Ou, J., Ball, J.M., Luan, Y., Zhao, T., Miyagishima, K.J., Xu, Y., Zhou, H., Chen, J., Merriman,
1032 D.K., Xie, Z., et al. (2018). iPSCs from a Hibernator Provide a Platform for Studying Cold
1033 Adaptation and Its Potential Medical Applications. *Cell* 173, 851-863.e16.
1034 <https://doi.org/10.1016/j.cell.2018.03.010>.

- 1035 7. Hendriks, K.D.W., Lupi, E., Hardenberg, M.C., Hoogstra-Berends, F., Deelman, L.E., and
1036 Henning, R.H. (2017). Differences in mitochondrial function and morphology during cooling
1037 and rewarming between hibernator and non-hibernator derived kidney epithelial cells.
- 1038 8. Anegawa, D., Sugiura, Y., Matsuoka, Y., Sone, M., Shichiri, M., Otsuka, R., Ishida, N.,
1039 Yamada, K., Suematsu, M., Miura, M., et al. (2021). Hepatic resistance to cold ferroptosis in
1040 a mammalian hibernator Syrian hamster depends on effective storage of diet-derived α -
1041 tocopherol. *Commun Biol* 4, 796. <https://doi.org/10.1038/s42003-021-02297-6>.
- 1042 9. Park, H.G., Han, S.I., Oh, S.Y., and Kang, H.S. (2005). Cellular responses to mild heat
1043 stress. *CMLS, Cell. Mol. Life Sci.* 62, 10–23. <https://doi.org/10.1007/s00018-004-4208-7>.
- 1044 10. Richter, K., Haslbeck, M., and Buchner, J. (2010). The Heat Shock Response: Life on the
1045 Verge of Death. *Molecular Cell* 40, 253–266. <https://doi.org/10.1016/j.molcel.2010.10.006>.
- 1046 11. Karunanithi, S., and Brown, I.R. (2015). Heat shock response and homeostatic plasticity.
1047 *Front. Cell. Neurosci.* 9. <https://doi.org/10.3389/fncel.2015.00068>.
- 1048 12. Kruuv, J., Glofcheski, D., Cheng, K.H., Campbell, S.D., Al-Qysi, H.M., Nolan, W.T., and
1049 Lepock, J.R. (1983). Factors influencing survival and growth of mammalian cells exposed to
1050 hypothermia. I. Effects of temperature and membrane lipid perturbers. *J Cell Physiol* 115,
1051 179–185. <https://doi.org/10.1002/jcp.1041150212>.
- 1052 13. Hochachka, P.W. (1986). Defense strategies against hypoxia and hypothermia. *Science*
1053 231, 234–241. <https://doi.org/10.1126/science.2417316>.
- 1054 14. Rule, G.S., Frim, J., Thompson, J.E., Lepock, J.R., and Kruuv, J. (1978). The effect of
1055 membrane lipid perturbers on survival of mammalian cells to cold. *Cryobiology* 15, 408–414.
1056 [https://doi.org/10.1016/0011-2240\(78\)90059-7](https://doi.org/10.1016/0011-2240(78)90059-7).
- 1057 15. Zachariassen, K.E. (1991). Hypothermia and cellular physiology. *Arctic Med Res* 50 *Suppl*
1058 6, 13–17.
- 1059 16. Heller, H.C., and Hammel, H.T. (1972). CNS control of body temperature during hibernation.
1060 *Comp Biochem Physiol A Comp Physiol* 41, 349–359. [https://doi.org/10.1016/0300-9629\(72\)90066-7](https://doi.org/10.1016/0300-9629(72)90066-7).
- 1062 17. Sunagawa, G.A., and Takahashi, M. (2016). Hypometabolism during Daily Torpor in Mice is
1063 Dominated by Reduction in the Sensitivity of the Thermoregulatory System. *Sci Rep* 6,
1064 37011. <https://doi.org/10.1038/srep37011>.
- 1065 18. Geiser, F. (2004). Metabolic rate and body temperature reduction during hibernation and
1066 daily torpor. *Annu Rev Physiol* 66, 239–274.
1067 <https://doi.org/10.1146/annurev.physiol.66.032102.115105>.
- 1068 19. Chayama, Y., Ando, L., Tamura, Y., Miura, M., and Yamaguchi, Y. (2016). Decreases in
1069 body temperature and body mass constitute pre-hibernation remodelling in the Syrian
1070 golden hamster, a facultative mammalian hibernator. *R Soc Open Sci* 3, 160002.
1071 <https://doi.org/10.1098/rsos.160002>.

- 1072 20. Park, K.J., Jones, G., and Ransome, R.D. (2000). Torpor, arousal and activity of hibernating
1073 Greater Horseshoe Bats (*Rhinolophus ferrumequinum*). *Functional Ecology* *14*, 580–588.
1074 <https://doi.org/10.1046/j.1365-2435.2000.t01-1-00460.x>.
- 1075 21. Cooper, S.T., Richters, K.E., Melin, T.E., Liu, Z., Hordyk, P.J., Benrud, R.R., Geiser, L.R.,
1076 Cash, S.E., Simon Shelley, C., Howard, D.R., et al. (2012). The hibernating 13-lined ground
1077 squirrel as a model organism for potential cold storage of platelets. *Am J Physiol Regul*
1078 *Integr Comp Physiol* *302*, R1202–R1208. <https://doi.org/10.1152/ajpregu.00018.2012>.
- 1079 22. Heldmaier, G., Ortman, S., and Elvert, R. (2004). Natural hypometabolism during
1080 hibernation and daily torpor in mammals. *Respiratory Physiology & Neurobiology* *141*, 317–
1081 329. <https://doi.org/10.1016/j.resp.2004.03.014>.
- 1082 23. Harris, R.A., Raveendran, M., Lyfoung, D.T., Sedlazeck, F.J., Mahmoud, M., Prall, T.M.,
1083 Karl, J.A., Doddapaneni, H., Meng, Q., Han, Y., et al. (2022). Construction of a new
1084 chromosome-scale, long-read reference genome assembly for the Syrian hamster,
1085 *Mesocricetus auratus*. *Gigascience* *11*, giac039.
1086 <https://doi.org/10.1093/gigascience/giac039>.
- 1087 24. Hart, T., Tong, A.H.Y., Chan, K., Van Leeuwen, J., Seetharaman, A., Aregger, M.,
1088 Chandrashekhar, M., Hustedt, N., Seth, S., Noonan, A., et al. (2017). Evaluation and Design
1089 of Genome-Wide CRISPR/SpCas9 Knockout Screens. *G3 (Bethesda)* *7*, 2719–2727.
1090 <https://doi.org/10.1534/g3.117.041277>.
- 1091 25. Mirabello, L., Macari, E.R., Jessop, L., Ellis, S.R., Myers, T., Giri, N., Taylor, A.M., McGrath,
1092 K.E., Humphries, J.M., Ballew, B.J., et al. (2014). Whole-exome sequencing and functional
1093 studies identify RPS29 as a novel gene mutated in multicase Diamond-Blackfan anemia
1094 families. *Blood* *124*, 24–32. <https://doi.org/10.1182/blood-2013-11-540278>.
- 1095 26. Summer, S., Smirnova, A., Gabriele, A., Toth, U., Fasemore, A.M., Förstner, K.U., Kuhn, L.,
1096 Chicher, J., Hammann, P., Mitulović, G., et al. (2020). YBEY is an essential biogenesis
1097 factor for mitochondrial ribosomes. *Nucleic Acids Res* *48*, 9762–9786.
1098 <https://doi.org/10.1093/nar/gkaa148>.
- 1099 27. Ni, M., Solmonson, A., Pan, C., Yang, C., Li, D., Notzon, A., Cai, L., Guevara, G., Zacharias,
1100 L.G., Faubert, B., et al. (2019). Functional Assessment of Lipoyltransferase-1 Deficiency in
1101 Cells, Mice, and Humans. *Cell Rep* *27*, 1376-1386.e6.
1102 <https://doi.org/10.1016/j.celrep.2019.04.005>.
- 1103 28. Xu, G., Li, W., Zhao, Y., Fan, T., Gao, Q., Wang, Y., Zhang, F., Gao, M., An, Z., and Yang,
1104 Z. (2024). Overexpression of Lias Gene Alleviates Cadmium-Induced Kidney Injury in Mice
1105 Involving Multiple Effects: Metabolism, Oxidative Stress, and Inflammation. *Biol Trace Elem*
1106 *Res* *202*, 2797–2811. <https://doi.org/10.1007/s12011-023-03883-x>.
- 1107 29. Douce, R., Bourguignon, J., Neuburger, M., and Rébeillé, F. (2001). The glycine
1108 decarboxylase system: a fascinating complex. *Trends Plant Sci* *6*, 167–176.
1109 [https://doi.org/10.1016/s1360-1385\(01\)01892-1](https://doi.org/10.1016/s1360-1385(01)01892-1).
- 1110 30. Weaver, K., and Skouta, R. (2022). The Selenoprotein Glutathione Peroxidase 4: From
1111 Molecular Mechanisms to Novel Therapeutic Opportunities. *Biomedicines* *10*, 891.
1112 <https://doi.org/10.3390/biomedicines10040891>.

- 1113 31. Seibt, T.M., Proneth, B., and Conrad, M. (2019). Role of GPX4 in ferroptosis and its
1114 pharmacological implication. *Free Radical Biology and Medicine* 133, 144–152.
1115 <https://doi.org/10.1016/j.freeradbiomed.2018.09.014>.
- 1116 32. Varlamova, E.G., Goltyaev, M.V., Novoselov, S.V., Novoselov, V.I., and Fesenko, E.E.
1117 (2013). Selenocysteine biosynthesis and mechanism of incorporation into growing proteins.
1118 *Mol Biol* 47, 488–495. <https://doi.org/10.1134/S0026893313040134>.
- 1119 33. French, R., and Simonovic, M. (2012). Synthesis and decoding of selenocysteine and
1120 human health. *Croatian medical journal* 53, 535–550.
1121 <https://doi.org/10.3325/cmj.2012.53.535>.
- 1122 34. Chen, T., Leng, J., Tan, J., Zhao, Y., Xie, S., Zhao, S., Yan, X., Zhu, L., Luo, J., Kong, L., et
1123 al. (2023). Discovery of Novel Potent Covalent Glutathione Peroxidase 4 Inhibitors as Highly
1124 Selective Ferroptosis Inducers for the Treatment of Triple-Negative Breast Cancer. *J. Med.*
1125 *Chem.* 66, 10036–10059. <https://doi.org/10.1021/acs.jmedchem.3c00967>.
- 1126 35. Shintoku, R., Takigawa, Y., Yamada, K., Kubota, C., Yoshimoto, Y., Takeuchi, T., Koshiishi,
1127 I., and Torii, S. (2017). Lipoxygenase-mediated generation of lipid peroxides enhances
1128 ferroptosis induced by erastin and RSL3. *Cancer Science* 108, 2187–2194.
1129 <https://doi.org/10.1111/cas.13380>.
- 1130 36. Sui, X., Zhang, R., Liu, S., Duan, T., Zhai, L., Zhang, M., Han, X., Xiang, Y., Huang, X., Lin,
1131 H., et al. (2018). RSL3 Drives Ferroptosis Through GPX4 Inactivation and ROS Production
1132 in Colorectal Cancer. *Front. Pharmacol.* 9. <https://doi.org/10.3389/fphar.2018.01371>.
- 1133 37. Hattori, K., Ishikawa, H., Sakauchi, C., Takayanagi, S., Naguro, I., and Ichijo, H. (2017).
1134 Cold stress-induced ferroptosis involves the ASK1-p38 pathway. *EMBO Rep* 18, 2067–
1135 2078. <https://doi.org/10.15252/embr.201744228>.
- 1136 38. Doll, S., Freitas, F.P., Shah, R., Aldrovandi, M., Da Silva, M.C., Ingold, I., Goya Grocin, A.,
1137 Xavier Da Silva, T.N., Panzilius, E., Scheel, C.H., et al. (2019). FSP1 is a glutathione-
1138 independent ferroptosis suppressor. *Nature* 575, 693–698. [https://doi.org/10.1038/s41586-](https://doi.org/10.1038/s41586-019-1707-0)
1139 [019-1707-0](https://doi.org/10.1038/s41586-019-1707-0).
- 1140 39. Bersuker, K., Hendricks, J.M., Li, Z., Magtanong, L., Ford, B., Tang, P.H., Roberts, M.A.,
1141 Tong, B., Maimone, T.J., Zoncu, R., et al. (2019). The CoQ oxidoreductase FSP1 acts
1142 parallel to GPX4 to inhibit ferroptosis. *Nature* 575, 688–692. [https://doi.org/10.1038/s41586-](https://doi.org/10.1038/s41586-019-1705-2)
1143 [019-1705-2](https://doi.org/10.1038/s41586-019-1705-2).
- 1144 40. Hu, Q., Wei, W., Wu, D., Huang, F., Li, M., Li, W., Yin, J., Peng, Y., Lu, Y., Zhao, Q., et al.
1145 (2022). Blockade of GCH1/BH4 Axis Activates Ferritinophagy to Mitigate the Resistance of
1146 Colorectal Cancer to Erastin-Induced Ferroptosis. *Front Cell Dev Biol* 10, 810327.
1147 <https://doi.org/10.3389/fcell.2022.810327>.
- 1148 41. Ma, T., Du, J., Zhang, Y., Wang, Y., Wang, B., and Zhang, T. (2022). GPX4-independent
1149 ferroptosis—a new strategy in disease’s therapy. *Cell Death Discov.* 8, 1–8.
1150 <https://doi.org/10.1038/s41420-022-01212-0>.
- 1151 42. Zhang, W., Dai, J., Hou, G., Liu, H., Zheng, S., Wang, X., Lin, Q., Zhang, Y., Lu, M., Gong,
1152 Y., et al. (2023). SMURF2 predisposes cancer cell toward ferroptosis in GPX4-independent

- 1153 manners by promoting GSTP1 degradation. *Molecular Cell* 83, 4352-4369.e8.
1154 <https://doi.org/10.1016/j.molcel.2023.10.042>.
- 1155 43. Sone, M., Mitsuhashi, N., Sugiura, Y., Matsuoka, Y., Maeda, R., Yamauchi, A., Okahashi,
1156 R., Yamashita, J., Sone, K., Enju, S., et al. (2023). Identification of genes supporting cold
1157 resistance of mammalian cells: lessons from a hibernator. Preprint at bioRxiv,
1158 <https://doi.org/10.1101/2023.12.27.573489> <https://doi.org/10.1101/2023.12.27.573489>.
- 1159 44. Davey, H.M., and Hexley, P. (2011). Red but not dead? Membranes of stressed
1160 *Saccharomyces cerevisiae* are permeable to propidium iodide. *Environ Microbiol* 13, 163–
1161 171. <https://doi.org/10.1111/j.1462-2920.2010.02317.x>.
- 1162 45. Kirchhoff, C., and Cypionka, H. (2017). Propidium ion enters viable cells with high
1163 membrane potential during live-dead staining. *Journal of Microbiological Methods* 142, 79–
1164 82. <https://doi.org/10.1016/j.mimet.2017.09.011>.
- 1165 46. Li, F.-J., Long, H.-Z., Zhou, Z.-W., Luo, H.-Y., Xu, S.-G., and Gao, L.-C. (2022). System Xc -
1166 /GSH/GPX4 axis: An important antioxidant system for the ferroptosis in drug-resistant solid
1167 tumor therapy. *Front Pharmacol* 13, 910292. <https://doi.org/10.3389/fphar.2022.910292>.
- 1168 47. Forman, H.J., Zhang, H., and Rinna, A. (2009). Glutathione: Overview of its protective roles,
1169 measurement, and biosynthesis. *Mol Aspects Med* 30, 1–12.
1170 <https://doi.org/10.1016/j.mam.2008.08.006>.
- 1171 48. Yoo, S.-E., Chen, L., Na, R., Liu, Y., Rios, C., Remmen, H.V., Richardson, A., and Ran, Q.
1172 (2012). Gpx4 ablation in adult mice results in a lethal phenotype accompanied by neuronal
1173 loss in brain. *Free Radic Biol Med* 52, 1820–1827.
1174 <https://doi.org/10.1016/j.freeradbiomed.2012.02.043>.
- 1175 49. Concordet, J.-P., and Haeussler, M. (2018). CRISPOR: intuitive guide selection for
1176 CRISPR/Cas9 genome editing experiments and screens. *Nucleic Acids Res* 46, W242–
1177 W245. <https://doi.org/10.1093/nar/gky354>.
- 1178 50. Stewart, S.A., Dykxhoorn, D.M., Palliser, D., Mizuno, H., Yu, E.Y., An, D.S., Sabatini, D.M.,
1179 Chen, I.S.Y., Hahn, W.C., Sharp, P.A., et al. (2003). Lentivirus-delivered stable gene
1180 silencing by RNAi in primary cells. *RNA* 9, 493–501. <https://doi.org/10.1261/rna.2192803>.
- 1181 51. Langmead, B., Trapnell, C., Pop, M., and Salzberg, S.L. (2009). Ultrafast and memory-
1182 efficient alignment of short DNA sequences to the human genome. *Genome Biol* 10, R25.
1183 <https://doi.org/10.1186/gb-2009-10-3-r25>.
- 1184 52. Li, W., Xu, H., Xiao, T., Cong, L., Love, M.I., Zhang, F., Irizarry, R.A., Liu, J.S., Brown, M.,
1185 and Liu, X.S. (2014). MAGeCK enables robust identification of essential genes from
1186 genome-scale CRISPR/Cas9 knockout screens. *Genome Biol* 15, 554.
1187 <https://doi.org/10.1186/s13059-014-0554-4>.
- 1188 53. R Core Team (2022). R: A Language and Environment for Statistical Computing |
1189 BibSonomy. R Foundation for Statistical Computing.
- 1190 54. Wei T, S.V. (2021). R package “corrplot”: Visualization of a Correlation Matrix (Version
1191 0.92). <https://github.com/taiyun/corrplot>.

1192 55. Silva, D., Santos, G., Barroca, M., and Collins, T. (2017). Inverse PCR for Point Mutation
1193 Introduction. In *PCR: Methods and Protocols Methods in Molecular Biology.*, L. Domingues,
1194 ed. (Springer), pp. 87–100. https://doi.org/10.1007/978-1-4939-7060-5_5.

1195

1196

1197

1198

1199

1200

1201

1202

1203

1204

1205

1206

1207

1208

1209

1210

1211

1212

1213

1214

1215

1216

1217

1218

1219

1220

1221

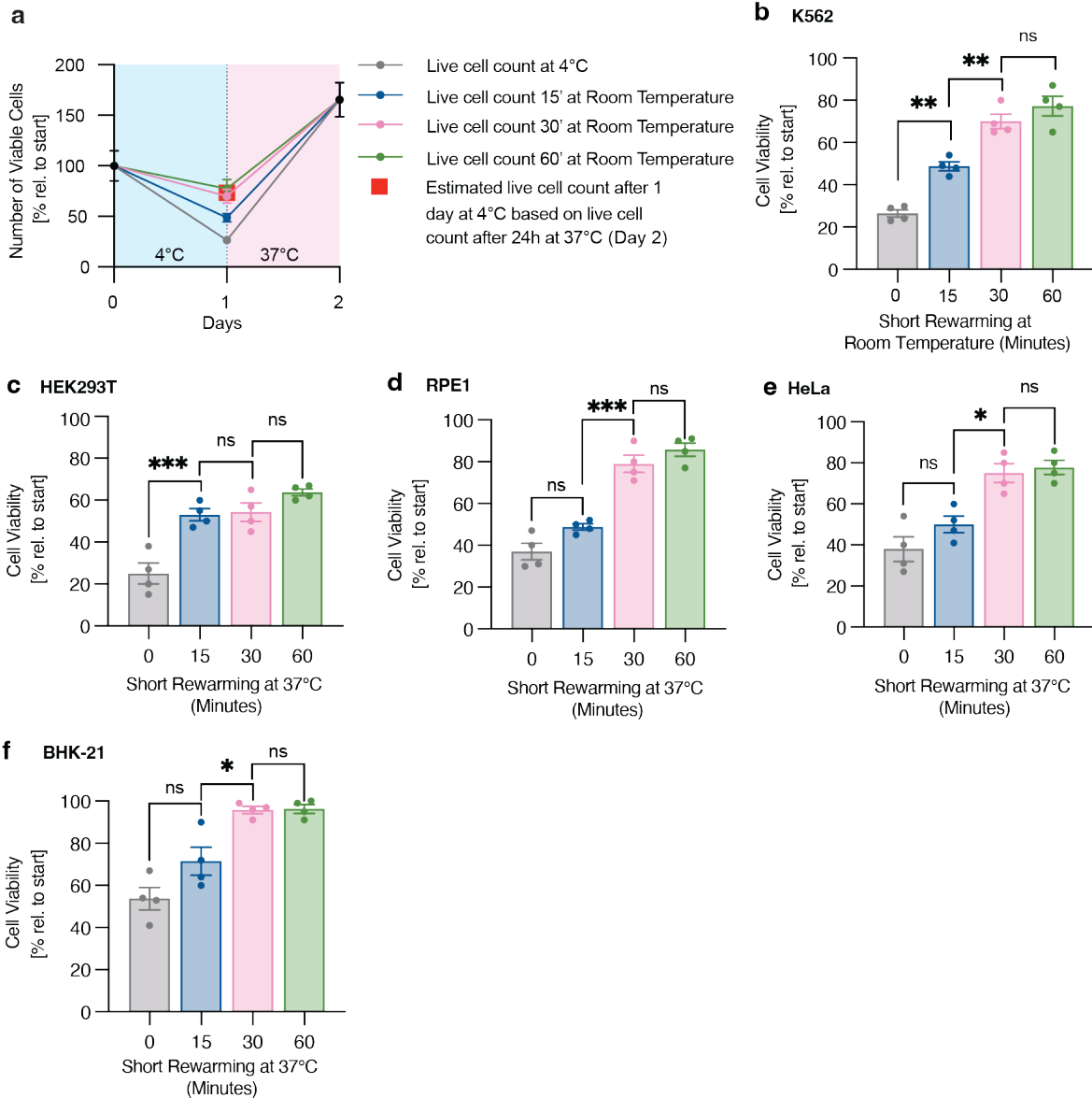
1222

1223

1224

1225

1226 Supplement



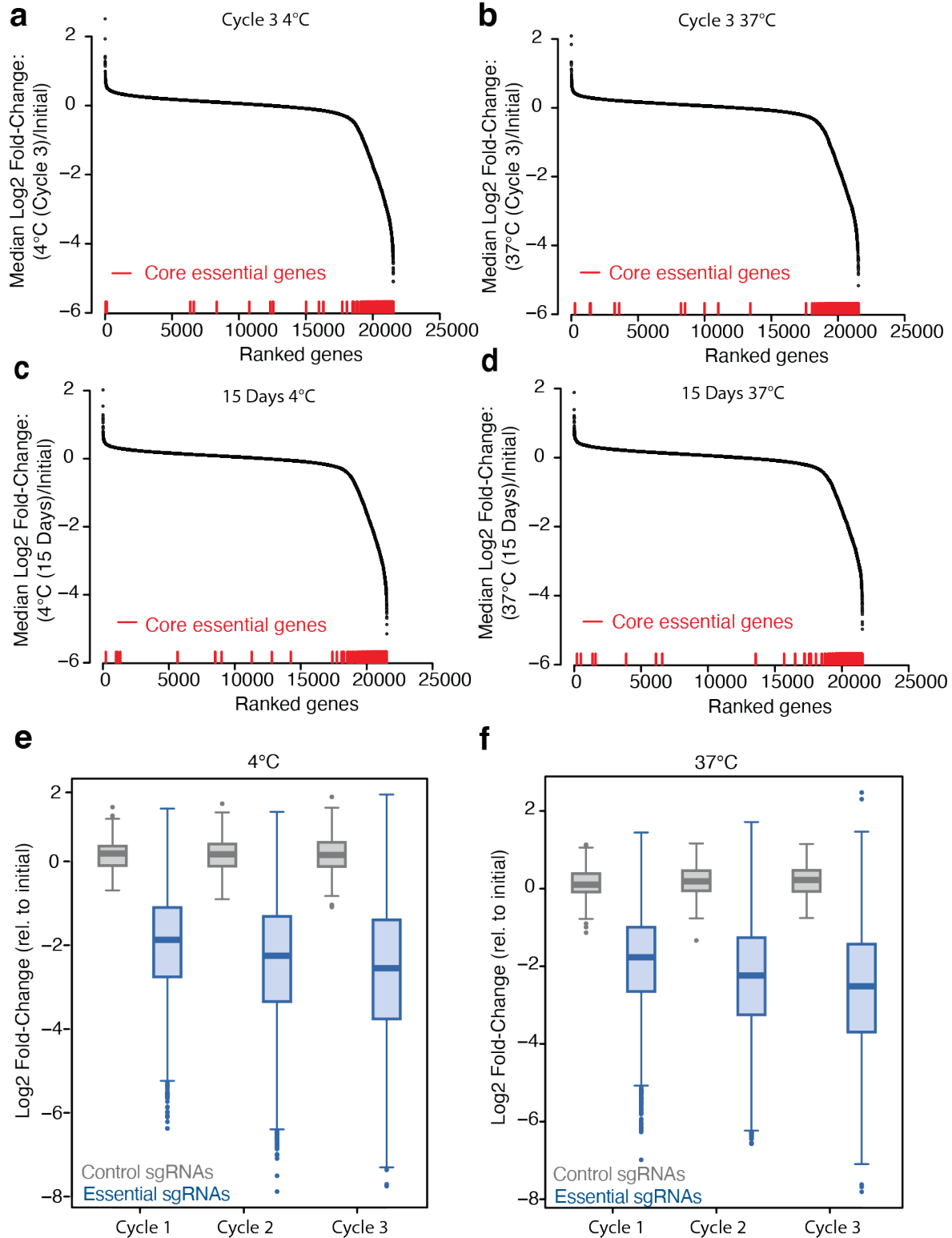
1227

1228

1229 **Supplement 1. Permeability to trypan blue changes rapidly upon cell rewarming**

1230 **a**, Number of viable K562 cells based on trypan blue staining after one day at 4°C and
 1231 subsequent rewarming for 24 hours at 37°C. Numbers are normalized to initial cell counts. Dots
 1232 indicate viable cell number based on trypan blue staining of cells after incubation at room
 1233 temperature for 15, 30, or 60 minutes. Blue shaded regions indicate 4°C exposure and shaded
 1234 pink regions indicate 37°C exposure. Red square indicates calculated cell counts after one day
 1235 at 4°C based on the viable cell number measured after 24 hour rewarming. **b**, Viability of K562
 1236 cells was assessed by trypan blue staining after incubation at room temperature for 0, 15, 30, or 80

1237 60 minutes following 24 hours at 4°C ($n = 4$). Cells incubated at room temperature for 15
1238 minutes show a significant increase in cell counts compared to cells counted immediately (** $P =$
1239 0.0016). Cells incubated at room temperature for 30 minutes show a significant increase in cell
1240 counts compared to a 15-minute incubation (** $P = 0.0023$), while no significant difference in
1241 viability was observed between cells incubated for 30 or 60 minutes (ns, $P = 0.4059$). **c-f**,
1242 Viability of cells was assessed by trypan blue staining after incubation at 37°C for 0, 15, 30, or
1243 60 minutes following 24 hours at 4°C ($n = 4$). **c**, HEK293T, **d**, RPE1, **e**, HeLa, **f**, BHK-21. No
1244 significant difference in cell viability was observed between cells incubated for 30 or 60 minutes
1245 for HEK293T (ns, $P = 0.3122$), RPE1 (ns, $P = 0.5137$), HeLa (ns, $P = 0.9735$), and BHK-21 (ns,
1246 $P = 0.9998$) cells. All values show mean \pm SEM, with significance determined by one-way
1247 ANOVA adjusted for multiple comparisons by Tukey's HSD. * $P < 0.05$; ** $P < 0.01$; *** $P < 0.001$;
1248 **** $P < 0.0001$; ns $P > 0.05$.
1249



1250

1251

Supplement 2. Depletion of Core Essential Genes in Genome-Wide BHK-21 Screens

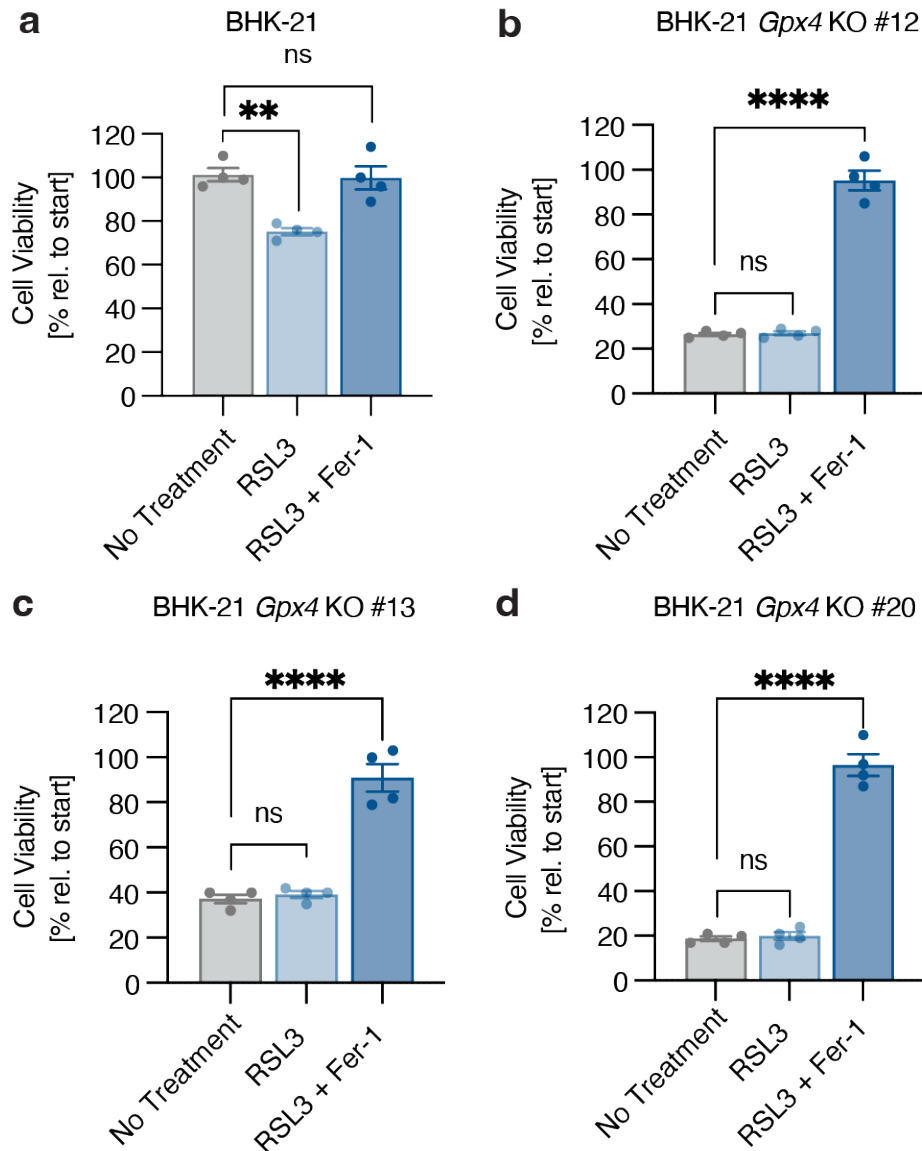
1252

a-d, Genes ranked by median fold-change (log₂) in genome-wide BHK-21 screens. **a**, after

1253

three cycles of cold exposure and rewarming (Cycle 3 4°C), **b**, matched constant 37°C control

1254 condition (Cycle 3 37°C), **c**, after 15 days of 4°C exposure (15 Days 4°C), **d**, matched constant
1255 37°C control condition (15 Days 37°C). Core essential genes²⁴ indicated in red are positioned
1256 below based on gene rank to demonstrate their depletion in each screen condition. **e-f**, Boxplots
1257 showing log₂ fold change in representation for the population of control sgRNAs (gray; n = 250)
1258 or sgRNAs targeting core essential genes²⁴ (blue; n = 4635) over **e**) three cycles of cold
1259 exposure and rewarming (4°C) or **f**) constant 37°C control conditions. The line within each box
1260 represents the median, the bounds of each box represent the first and third quartiles, and the
1261 whiskers extend to the furthest data point within 1.5 times the interquartile range. A two-sided
1262 Kolmogorov-Smirnov test was used to test the difference between each pair of control/essential-
1263 gene-targeting sgRNA distributions (estimated p-value < 2.2e-16 for all six pairs in e and f).
1264



1265

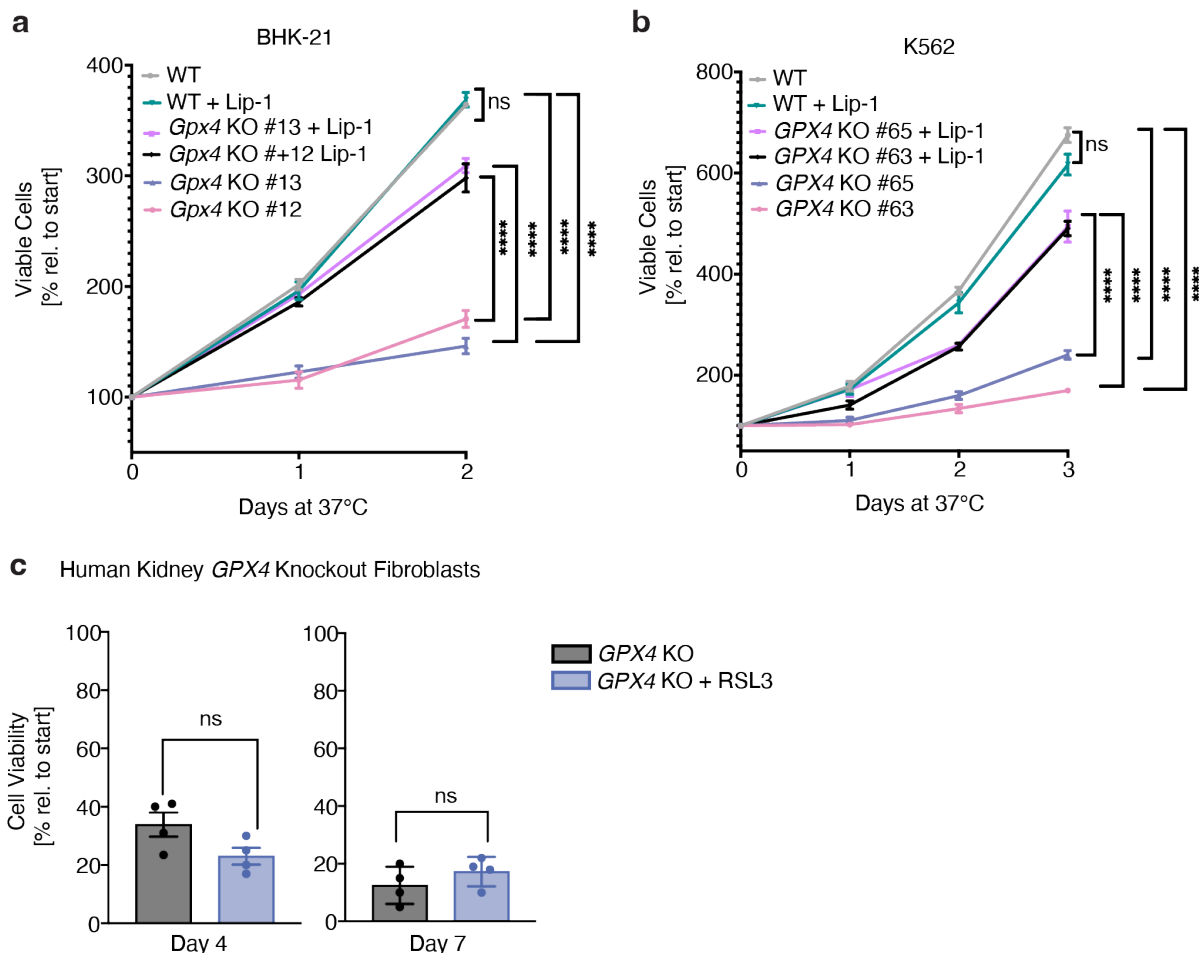
1266

1267 **Supplement 3. RSL3 treatment has no effect on the viability of cold-exposed *Gpx4* KO**

1268 **BHK-21 cells.**

1269 **a-d**, Wild-type BHK-21 cells (**a**) and three independent *Gpx4* KO BHK-21 clonal lines (**b-d**) were
1270 treated with RSL3 (1 μ M) and ferrostatin-1 (Fer-1, 1 μ M) as indicated for 24 hours at 4°C ($n = 4$)
1271 prior to trypan blue staining. Wild-type BHK-21 cells show a significant decrease in cell viability
1272 when treated with RSL3 compared to no treatment (** $P = 0.0013$), whereas *Gpx4* KO lines
1273 show no significant changes in viability (ns, $P > 0.05$). All values show mean \pm SEM, with
1274 significance measured by one-way ANOVA adjusted for multiple comparisons by Dunnett's test.

1275 * $P < 0.05$; ** $P < 0.01$; *** $P < 0.001$; **** $P < 0.0001$; ns $P > 0.05$.



1276

1277 **Supplement 4. Growth of BHK21 and K562 GPX4 knockout cells and effects of RSL3**

1278 **treatment on human kidney fibroblast GPX4 knockout cells**

1279 **a**, Viable K562 cells recorded as percentage relative to start based on trypan blue staining over

1280 the course of 3 days at 37°C. Cell growth is significantly decreased in GPX4 K562 KO clones

1281 compared to WT K562 cells. Supplementation of lipoxstatin-1 (2.5 μM) increases cell viability in

1282 GPX4 KO cells and not WT cells at 37°C. **b**, Viable BHK-21 cells recorded as percentage

1283 relative to start based on trypan blue staining over the course of 2 days. Cell growth is

1284 significantly decreased in *Gpx4* BHK-21 KO cells compared to WT BHK-21 cells.

1285 Supplementation of lipoxstatin-1 (2.5 μM) increases cell viability in *Gpx4* KO cell and not WT

1286 cells at 37°C. **c**, Human kidney GPX4 KO cells were placed at 4°C and left untreated or treated

1287 with RSL3 (1 μM) for 4, and 7 days (n = 4). Treatment with RSL3 does not confer significant

1288 additional death (n=4 per timepoint and condition) as measure by two-tailed t-test. All values

1289 show mean ± SEM, with significance measured by one-way ANOVA adjusted for multiple

1290 comparisons with Tukey's HSD unless otherwise specified. * $P < 0.05$; ** $P < 0.01$; *** $P < 0.001$;
1291 **** $P < 0.0001$; ns $P > 0.05$.

1292

1293

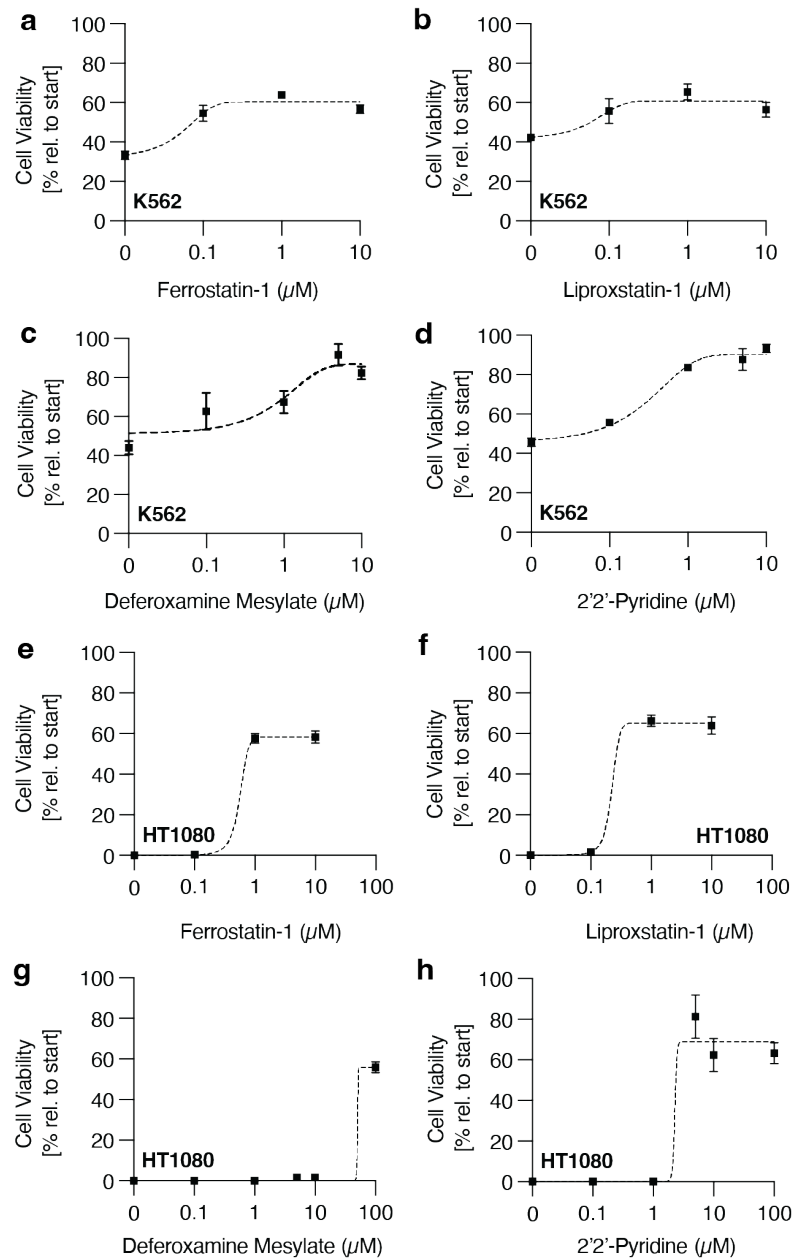
1294

1295

1296

1297

1298



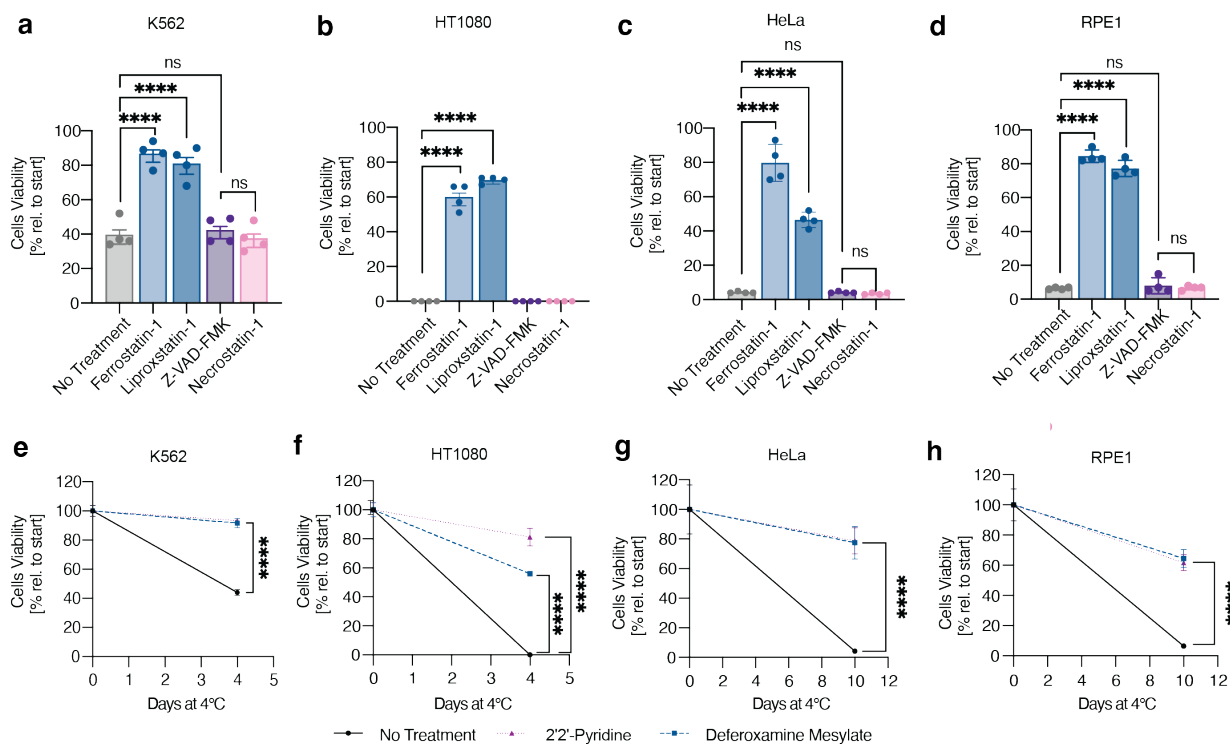
1299

1300

1301 **Supplement 5. Ferroptosis inhibitors and iron chelators increase cold cell viability in a**
1302 **dose-dependent manner**

1303 **a-h**, K562 (**a-d**) and HT1080 (**e-h**) cells were treated with varying concentrations of the
1304 ferroptosis inhibitors, ferrostatin-1 and liproxstatin-1, and iron chelators, deferoxamine and 2'2'-
1305 pyridine, for four days at 4°C prior to assaying cell viability by trypan blue staining ($n = 3$). All
1306 values show mean \pm SEM.

1307



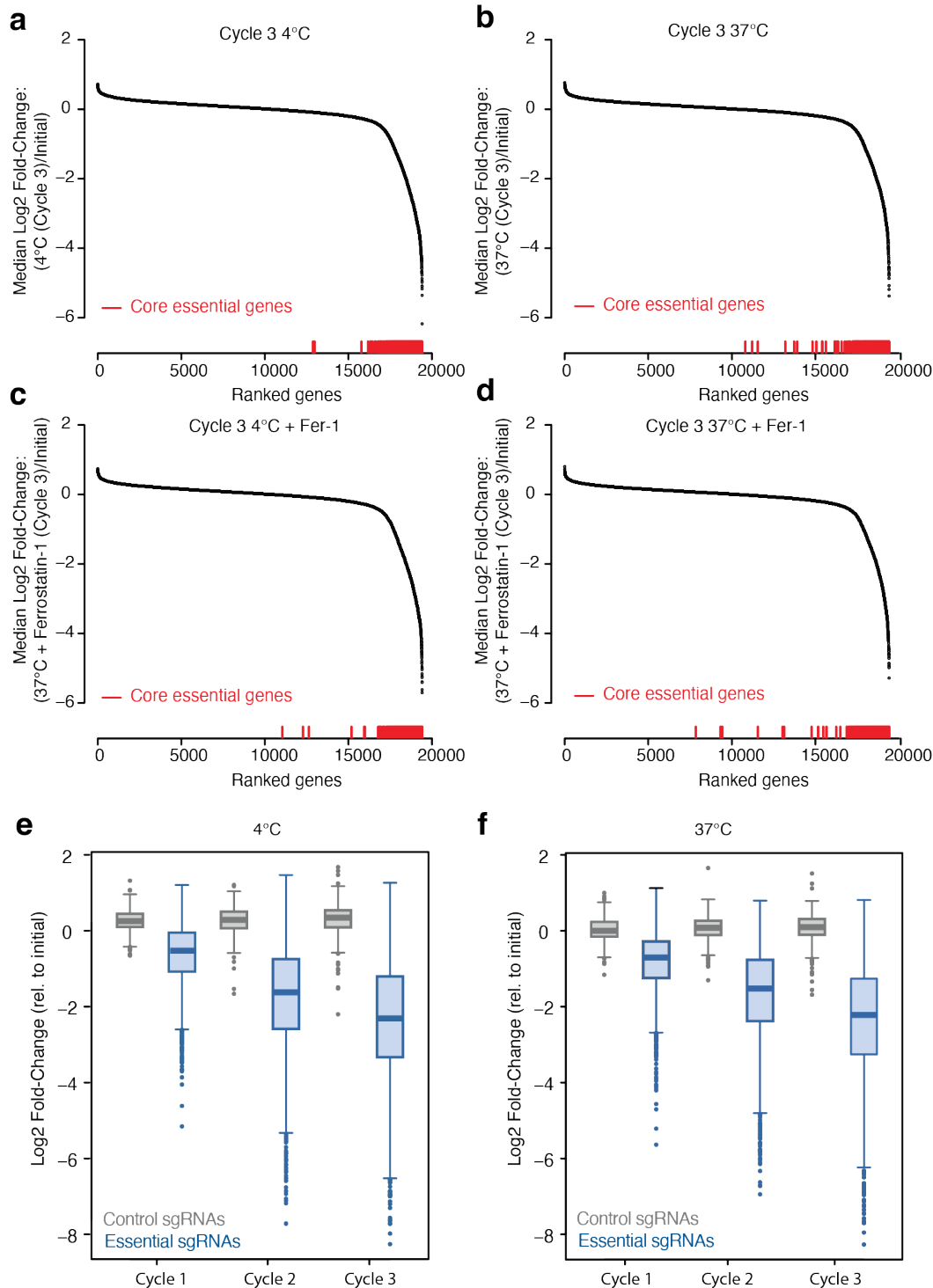
1308

1309

1310 **Supplement 6. Cells derived from non-hibernators undergo cold-induced ferroptotic cell**
 1311 **death**

1312 **a**, K562 cells were treated with ferrostatin-1 (1 μM) (**** $P < 0.0001$), liproxstatin-1 (1 μM) (**** $P < 0.0001$),
 1313 Z-VAD-FMK (1 μM) (ns, $P = 0.9760$), or necrostatin-1 (1 μM) (ns, $P = 0.9835$) for 4
 1314 days at 4°C prior to trypan blue staining ($n = 4$). **b**, HT1080 cells treated with ferrostatin-1 (1 μM)
 1315 (**** $P < 0.0001$), liproxstatin-1 (1 μM) (**** $P < 0.0001$), Z-VAD-FMK (1 μM), or necrostatin-1 (1
 1316 μM) for 4 days at 4°C prior to trypan blue staining ($n = 4$). **c**, HeLa cells treated with ferrostatin-1
 1317 (1 μM) (**** $P < 0.0001$), liproxstatin-1 (1 μM) (**** $P < 0.0001$), Z-VAD-FMK (1 μM) (ns, $P >$
 1318 0.9999), or necrostatin-1 (1 μM) (ns, $P = 0.9987$) for 10 days at 4°C prior to trypan blue staining
 1319 ($n = 4$). **d**, RPE1 cells treated with ferrostatin-1 (1 μM) (**** $P < 0.0001$), liproxstatin-1 (1 μM)
 1320 (**** $P < 0.0001$), Z-VAD-FMK (1 μM) (ns, $P = 0.9291$), or necrostatin-1 (1 μM) (ns, $P > 0.9999$)
 1321 for 10 days at 4°C prior to trypan blue staining ($n = 4$). **e**, K562 cells treated with deferoxamine
 1322 mesylate (5 μM) (** $P = 0.0002$) or 2'2'-pyridine (10 μM) (**** $P < 0.0001$) for 4 days at 4°C prior
 1323 to trypan blue staining ($n = 3$). **f**, HT1080 cells treated with deferoxamine mesylate (100 μM)
 1324 (**** $P < 0.0001$) or 2'2'-pyridine (5 μM) (** $P = 0.0002$) for 4 days at 4°C prior to trypan blue
 1325 staining ($n = 3$). **g**, HeLa cells treated with deferoxamine mesylate (5 μM) (**** $P < 0.0001$) or
 1326 2'2'-pyridine (5 μM) (**** $P < 0.0001$) for 10 days at 4°C prior to trypan blue staining ($n = 3$). **h**,

1327 RPE1 cells treated with deferoxamine mesylate (100 μ M) (**** $P < 0.0001$) or 2'2'-pyridine (5
1328 μ M) (*** $P < 0.0001$) for 10 days at 4°C prior to trypan blue staining ($n = 3$). All values show
1329 mean \pm SEM, with significance measured one-way ANOVA adjusted for multiple comparisons
1330 by Dunnett's test. * $P < 0.05$; ** $P < 0.01$; *** $P < 0.001$; **** $P < 0.0001$; ns $P > 0.05$.
1331



1332

1333

1334 Supplement 7. Depletion of Core Essential Genes in Genome-Wide K562 Screens

1335 **a-d**, Genes ranked by median fold-change (log₂) in genome-wide K562 screens. **a**, after three

1336 cycles of cold exposure (Cycle 3 4°C), **b**, matched constant 37°C control condition (Cycle 3

1337 37°C), **c**, three cycles of cold exposure with 1 μ M ferrostatin-1 (Cycle 3 4°C + Fer-1), **d**,
1338 matched constant 37°C control condition with 1 μ M ferrostatin-1 (Cycle 3 37°C + Fer-1). Core
1339 essential genes²⁴ (red bars) are positioned below based on gene rank to demonstrate their
1340 depletion in each screen condition. **e-f**, Boxplots showing the log₂ fold change in representation
1341 for the population of control sgRNAs (gray; n = 500) or sgRNAs targeting core essential genes²⁴
1342 (blue; n = 3219) over **e**) three cycles of cold exposure (4°C) or **f**) constant 37°C control
1343 conditions. The line within each box represents the median, the bounds of each box represent
1344 the first and third quartiles, and the whiskers extend to the furthest data point within 1.5 times
1345 the interquartile range. A two-sided Kolmogorov-Smirnov test was used to test the difference
1346 between each pair of control/essential-gene-targeting sgRNA distributions (estimated p-value <
1347 2.2e-16 for all six pairs in e and f).

1348

1349

1350

1351

1352

1353

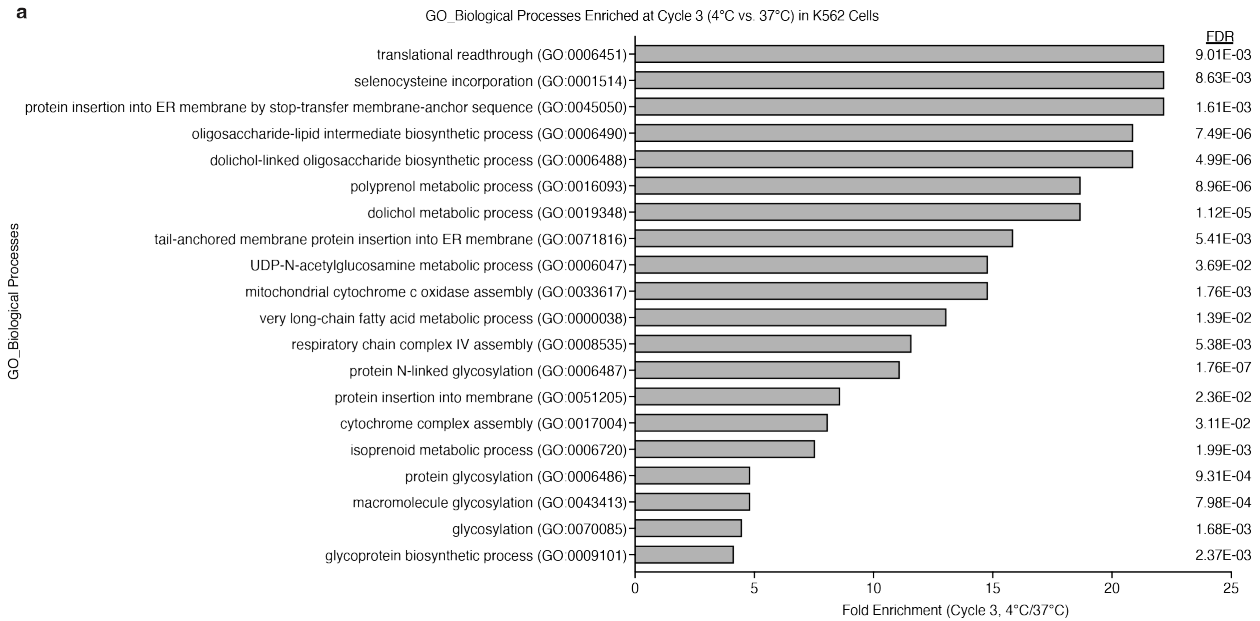
1354

1355

1356

1357

1358



1359

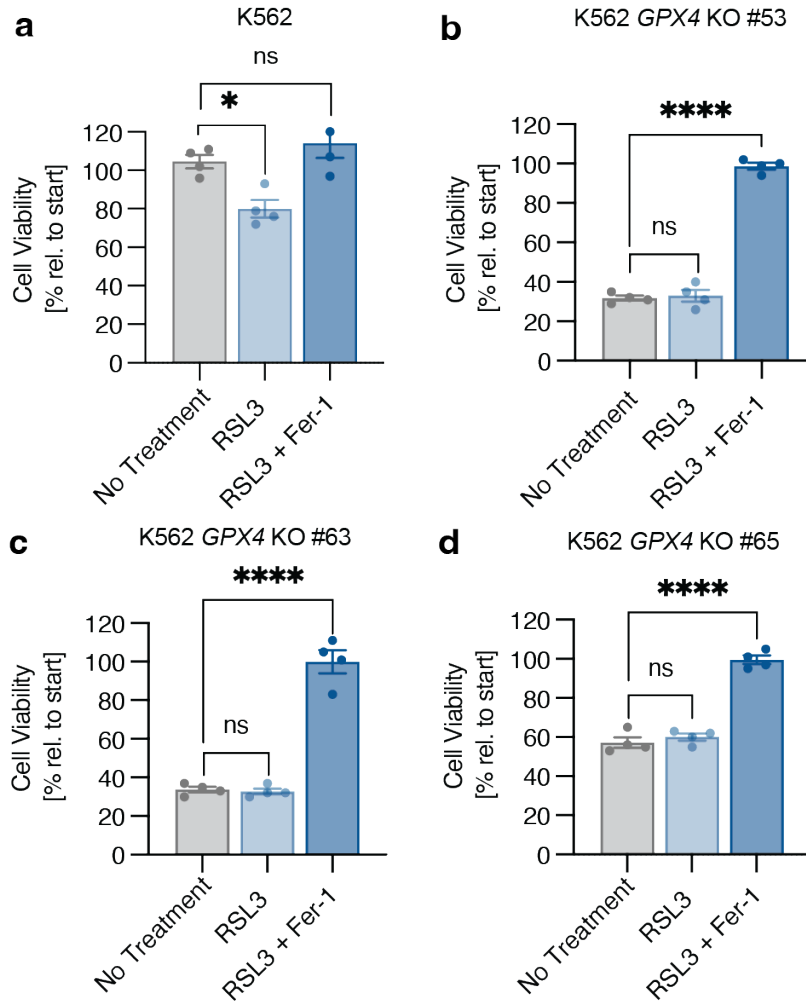
1360

1361 **Supplement 8. Top 20 enriched pathways at Cycle 3 (4°C vs. 37°C) in K562 cells**

1362 **a**, Graphical representation of the top 20 enriched, differentially expressed gene sets (204
 1363 genes; FDR < 0.1) from the genome-scale CRISPR-Cas9 screen in K562 cells (Cycle 3 4°C vs.
 1364 3 passages at 37°C). GO_Biological Processes Panther overrepresentation test was used to
 1365 determine enriched gene sets. Functional annotation analysis of the selectively required genes
 1366 identified pathways related to translational readthrough, selenocysteine incorporation, protein
 1367 insertion into the ER, glycosylation, fatty acid metabolism, and mitochondrial respiration. A full
 1368 list of pathways is provided in Table S6.

1369

1370



1371

1372

1373 **Supplement 9. RSL3 treatment has no effect on the viability of cold-exposed GPX4 KO**

1374 **K562 cells.**

1375 **a-d,** Wild-type K562 cells (**a**) and three independent GPX4 KO K562 clonal lines (**b-d**) were

1376 treated with RSL3 (1 μ M) and ferrostatin-1 (Fer-1, 1 μ M) as indicated for 8 hours at 4°C ($n = 4$)

1377 prior to trypan blue staining. Wild-type K562 cells show a significant decrease in cell viability

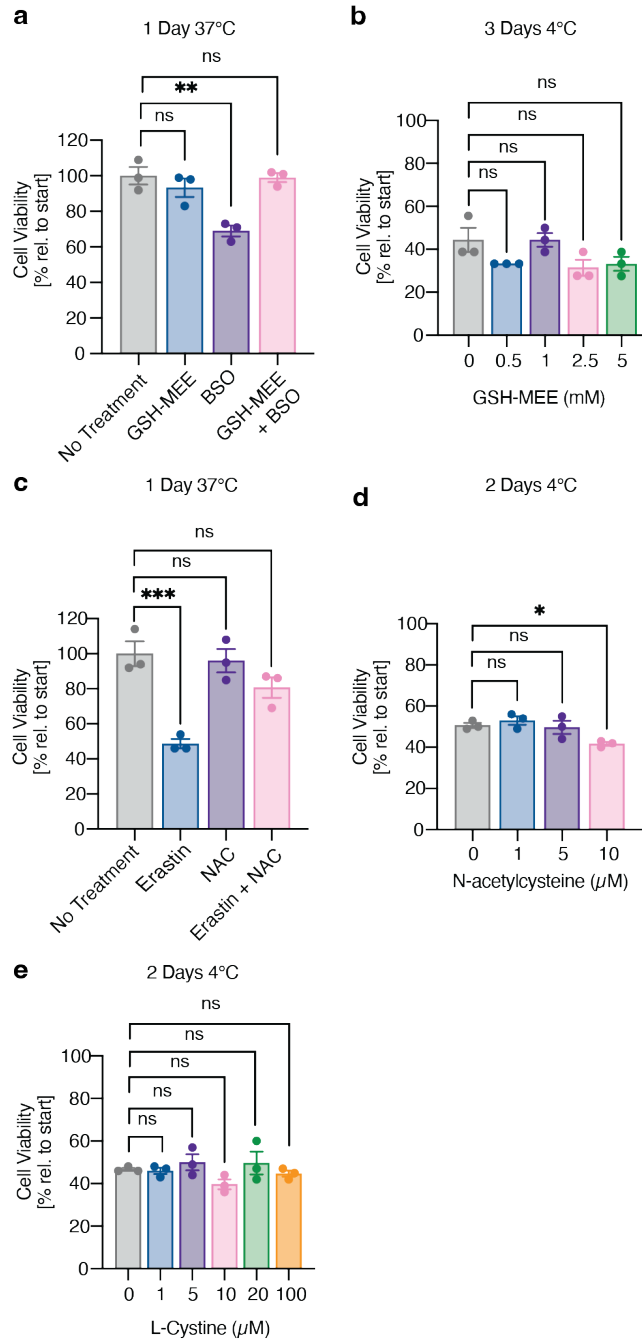
1378 when treated with RSL3 compared to no treatment (* $P = 0.0213$), whereas GPX4 KO lines show

1379 no significant changes in viability (ns, $P > 0.05$). All values show mean \pm SEM, with significance

1380 measured by one-way ANOVA adjusted for multiple comparisons by Dunnett's test. * $P < 0.05$;

1381 ** $P < 0.01$; *** $P < 0.001$; **** $P < 0.0001$; ns $P > 0.05$.

1382



1383

1384

1385 **Supplement 10. Cell permeable glutathione and glutathione precursors do not increase**
 1386 **cold cell viability**

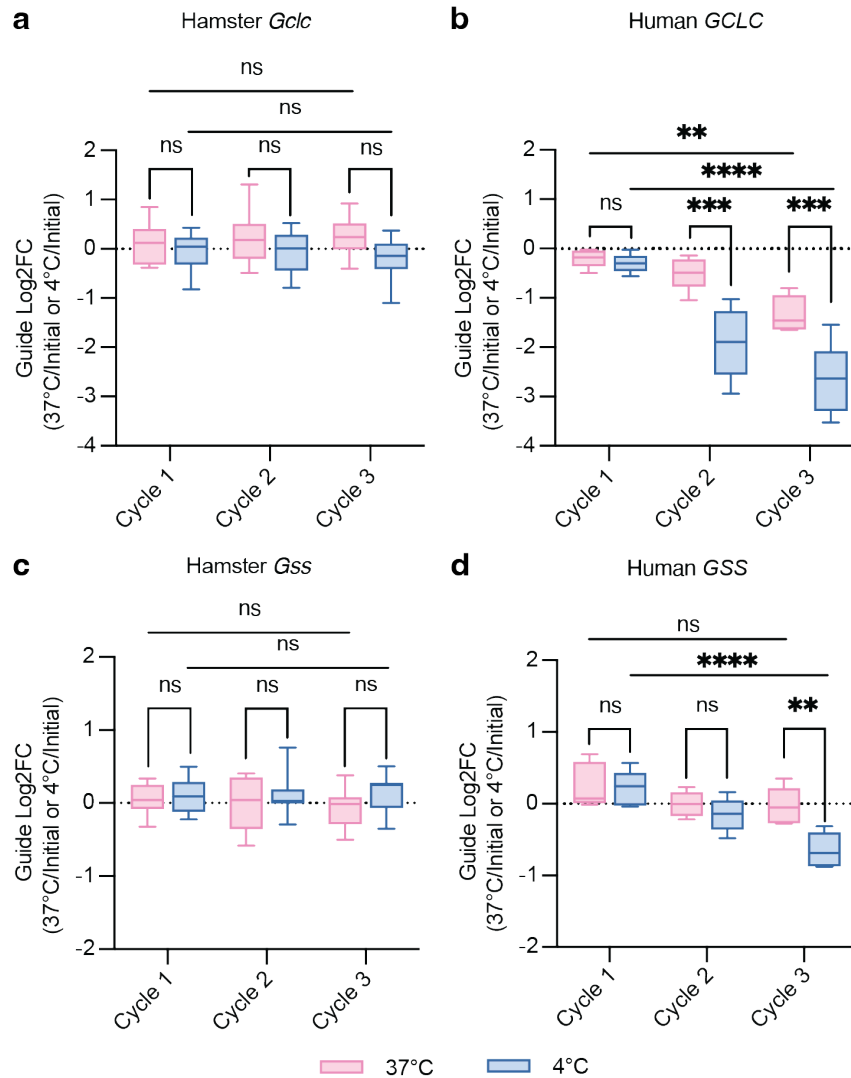
1387 **a**, K562 cells were placed at 37°C and treated with cell permeable glutathione GSH-MEE (1 μM)
 1388 and/or the glutathione synthesis inhibitor buthionine sulfoximine (BSO, 1 μM) for 1 day ($n = 3$).
 1389 Treatment with BSO resulted in increased cell death (** $P = 0.0018$) that was rescued by GSH-
 1390 MEE (ns, $P = 0.9961$). **b**, Treatment with GSH-MEE has no effect on K562 cold-induced death

1391 after 3 days at 4°C as measured by trypan blue staining ($n = 3$, 5 μM ; ns, $P = 0.1558$). **c**, K562
1392 cells were placed at 37°C and treated with ferroptosis inducer Erastin (10 μM) and N-
1393 acetylcysteine (NAC, 10 μM) for 1 day ($n = 3$). Treatment with Erastin resulted in increased cell
1394 death ($***P = 0.0006$) that was rescued by NAC (ns, $P = 0.1091$). **d**, Treatment with N-
1395 acetylcysteine does not increase cold cell viability in K562 cells after 2 days at 4°C as measured
1396 by trypan blue staining ($n = 3$, 10 μM ; $*P = 0.0352$). **e**, Treatment with L-Cystine does not
1397 increase cold cell viability in K562 cells after 2 days at 4°C as measured by trypan blue staining
1398 ($n = 3$, 100 μM ; ns, $P = 0.9843$). All values show mean \pm SEM, with significance measured by
1399 one-way ANOVA adjusted for multiple comparisons by Dunnett's test. $*P < 0.05$; $**P < 0.01$;
1400 $***P < 0.001$; $****P < 0.0001$; ns $P > 0.05$.

1401

1402

1403



1404

1405

1406 **Supplement 11. Glutathione biosynthesis genes show increased depletion in cold-**
 1407 **exposed K562 cells**

1408 **a,c**, Log₂ fold-change (log₂FC) of 10 guides per targeted gene in BHK-21 genome-wide screen,
 1409 showing guide depletion over three cycles of cold exposure and rewarming. **a**, *Glc*, **c**, *Gss*. **b**,

1410 **d**, Log₂ fold-change (log₂FC) of 5 guides per targeted gene in K562 genome-wide screen,
 1411 showing significant guide depletion over three cycles of cold exposure. **b**, *GCLC*, **d**, *GSS*.

1412 Significance between Cycle 1 versus Cycle 3 is measured by two-way ANOVA adjusted for

1413 multiple comparisons by Dunnett's test. Significance between 37°C and 4°C for each cycle is

1414 measured by two-way ANOVA adjusted for multiple comparisons by Bonferroni's test. **P* < 0.05;

1415 ***P* < 0.01; ****P* < 0.001; *****P* < 0.0001; ns *P* > 0.05.

1416